SANS STUDY OF MOLECULAR-COLLOIDAL SOLUTIONS OF C_{60} FULLERENES IN WATER

M.V.Avdeev[1], V.L.Aksenov[1], G.V.Andrievsky[2], L.I.Derevyanchenko[2], V.K.Klochkov[2], A.A.Khokhryakov[1,3]

[1]*Frank Laboratory of Neutron Physics, JINR, Dubna, Russia*
[2]*Institute for Therapy of Ukrainian AMS , Kharkov, Ukraine*
[3] *Kyiv Taras Shevchenko National University, Kyiv, Ukraine*

Since the discovery of fullerenes (1985) their biological activity was a question of particular interest. As a consequence, biological effects of fullerenes were actively studied for the last 10 years. This kind of investigations is connected mainly with the so-called "water-soluble" fullerenes — hydrophilic chemical derivatives of fullerenes. This approach was determined by a commonly accepted opinion that fullerenes are typical hydrophobic molecules and cannot form true solutions in water. However, starting from 1994 Andrievsky G.V and co-workers developed [1,2] a method of fabricating aqueous molecular-colloidal solutions of C_{60} fullerene (C_{60}FWS) with the properties of both true and colloidal solutions simultaneously. This method is based on the transferring of fullerene from an organic solution into the aqueous phase with the help of ultrasonic treatment. The resulting dispersion is stable and has a significant therapeutic effect when treating experimental pathologies [3,4]. The mechanism of this effect is assumed to be quite different from that of other antioxidants.

In the present work the small-angle neutron scattering (SANS) is applied to study the structure of C_{60}FWS which was produced without resort to any solubilizers and chemical modification. The aim of the experiments was to clarify the mechanism of stabilization for C_{60}FWS basing on the information about the inner structure of the colloids. Experiments were carried out on the YuMO setup at the IBR-2 pulsed reactor at room temperature (20^{o}C). The scattering curves were obtained in a q-interval 0.007÷0.15 Å^{-1}. In the studied samples of C_{60}FWS the C_{60} concentration was from 0.002 to 0.2 mM (0.0014÷0.14 mg/ml). Experiments were repeated twice for samples of different time preparation and showed a full reproducibility.

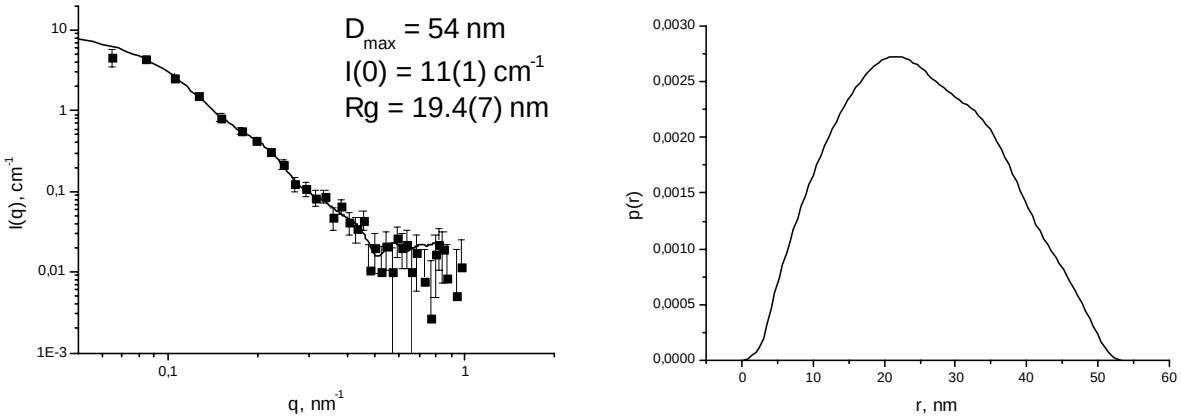

a) *b*)

Fig.1. Typical small-angle neutron scattering curve (a) and the pare distance distribution function (b) for C_{60}FWS, c = 0.192 mM, T = 20^{o}C.

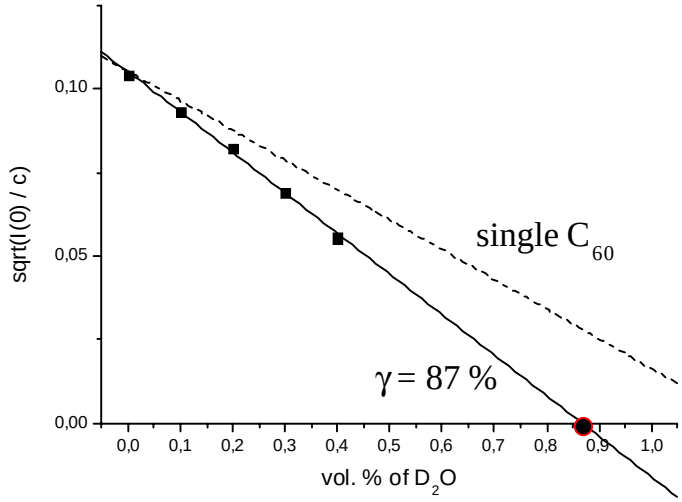

Fig. 2. Contrast variation for C_{60}FWS, c = 0.192 mM, T = 20°C; γ is the match point of the system corresponding to relative content of D_2O when the scattering from the aggregates disappears. Dashed line corresponds to behavior of the contrast as if fullerenes are single.

The SANS curves (Fig.1) show that these systems are highly polydisperse in a wide scale interval up to 50 nm, which testifies the electron microscopy data [5]. The attempts to obtain the stable size distribution function of aggregates using the uniform spherical form-factors fail. Along with it the contrast variation (Fig.2) performed by diluting C_{60}FWS with heavy water points to the presence of a component in the aggregates, which is different from fullerenes and is assumed to be responsible for the stabilization of the solutions. The origin of this component, in particular the hypothesis about the formation of a specific hydration shell around fullerenes [2], is under discussion now. It should be pointed out that in general the structure of the studied systems is very close to that of the system C_{60}/pyridine/water where the role of stabilizer plays a thin pyridine shell around fullerene complexes [6, 7]. Also, the structural changes after the coagulation which takes place in the solutions on addition of salts were determined and are under analysis at the moment.

The work was carried out with the support of the Russian Ministry of Industry, Science and Technologies, state contract №40.012.1.1.1148.

References

1. G.V. Andrievsky et al., J. Chem. Soc., Chem. Commun. 12 (1995) 1281.
2. G.V. Andrievsky et al., Chem. Phys. Lett. 364 (2002) 8; and UA patent N29540 of 11/15/2000.
3. A.D. Roslyakov, et.al., Zh. Akad. Med. Nauk Ukrainy. 5 (1999) 338 (in Russian).
4. G.V. Andrievsky, I.S. Burenin. In "On Medicinal And Preventive Efficacy Of Small Doses Of Hydrated C_{60} Fullerenes At Cancer Pathologies". Chemistry Preprint Server: http://preprint.chemweb.com/medichem/0206001. ChemWeb.com News Bulletin, 11 June, 2002.
5. G.V. Andrievsky et al., Chem. Phys. Lett. 300 (1999) 392
6. V.L.Aksenov, M.V.Avdeev, et al., In "Electronic properties of novel materials – molecular nanostructures", Eds. H.Kuzmany, J.Fink, M.Mehring, S.Roth, AIP Conference Proceedings, 591 (2002) 66
7. V.L. Aksenov, M.V. Avdeev, A.A. Timchenko, I.N. Serdyuk, R.P. May In “Frontiers of Multifunctional Nanosystems”, Eds. E. Buzaneva and P. Scharff, Kluewer Academic Publishers: Netherlands, (2002) 281

FROM SANS INVESTIGATIONS OF MECHANISM OF A MEMBRANE PROTEIN CRYSTALLIZATION TO A MOLECULAR BASIS FOR TRANSCELL SIGNALLING

V.Gordeliy [1, 2, 3], R.Efremov [2, 3], R.Moukhametzianov [2, 3], G.Bobarykina [2], A.Islamov[2], A.Kuklin[2], J.Klare [4], M.Engelhard [4], G.Bueldt [2]

[1]*Frank Laboratory of Neutron Physics, Joint Institute for Nuclear Research, Dubna, Russia,*
[2]*Institute of Structural Biology, Forschungszentrum, Juelich, Germany*
[3]*Centre of Biophysics and Physical Chemistry of Supramolecular Structures, Moscow Institute of Physics and Technology, Dolgoprudny, Russia,*
[4]*Max Planck Institut für Molekulare Physiologie, Dortmund, Germany*

Membrane proteins, residing in lipid bilayers are responsible for vital processes in the cells such as transformation of energy, solute transport, charge separation as well as signal transduction. Understanding of such fundamental processes at a molecular level requires knowledge of the structures of these proteins at high resolution. Crystallographic methods need well-ordered three-dimensional crystals, but it is extremely difficult to obtain proteins of this class in suitable crystalline forms.

Landau and Rosenbush proposed a novel approach for crystallizing membrane proteins in a lipidic cubic phase (Landau *et al*., 1996). This system, consisting of lipid, water and protein in appropriate proportions, forms a structured, transparent and complex three-dimensional lipidic array, which is pervaded by an intercommunicating aqueous channel bicontinuous system. Such matrices provide nucleation sites and support growth of the crystals. This method of crystallization in the cubic phase was successful in the crystallization of an important membrane protein - bacteriorhodopsin (BR) (Pebay-Peyroula *et al*., 1997). However, it was not clear whether the crystallization of membrane proteins in the lipidic cubic phase is a general method. Moreover, in spite of the attempts to study its mechanism of crystallization (Nollert *et al*., 2001; Caffrey, 2000), it is an open problem why the lipidic cubic phase promotes the crystallization of the membrane proteins.

One of main aims of this work was to study in detail the kinetics of phase behaviour of protein/lipid cubic phase/buffer system (proteolipidic cubic phase) in the course of BR crystallization. This investigation is necessary to understand how general is the behaviour of the cubic phase in those cases where BR crystals grow and to answer the question about necessity of phase transitions for protein crystallization, since it was believed that the phase transition could be a key step in the crystallisation. In the present work detailed kinetics of the proteolipidic cubic phase behaviour was studied by SANS at small angle neutron scattering spectrometer YuMO (FLNP, JINR, Dubna, Russia) in the range from 0.01 $Å^{-1}$ to 0.4 $Å^{-1}$ ($Q=4\pi \sin\theta/\lambda$) at the standard crystallization conditions (Landau *et al*., 1996). It was found that in spite of significant influence of the protein on parameters of the lipid cubic phase caused by salt addition (Fig.1), the Pn3m symmetry of the cubic phase -monooleoyl-*rac*-glycerol (monoolein, C18:1c9) remains unchanged during the entire crystallization process. It was shown that coexistence of the “macroscopic” amount of the other phases as well as the presence of a phase transition is not necessary for the crystallization process (Gordeliy et al., 2002, Bobarikina et.al, 2002).

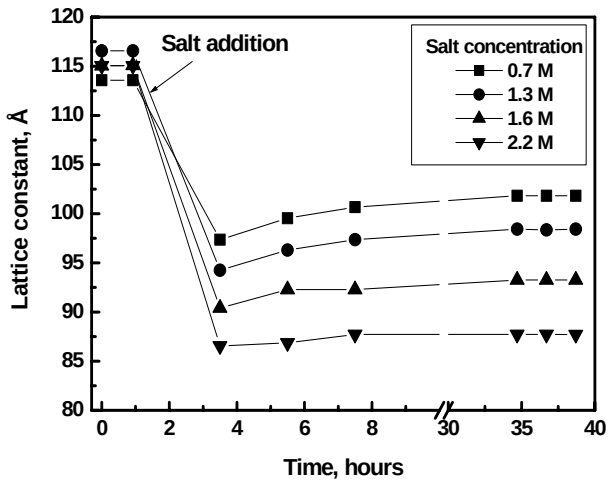

Fig.1. The time dependence of the lattice constant of MO/BR/buffer system at different salt concentrations. The arrow shows the moment of the salt addition, which leads to significant changes of the lattice constant. The decrease of the lattice constant depends on the salt concentration.

Thus, the presence of the macroscopic amount of an additional phase as well as a phase transition are not necessary conditions for the crystallization of BR molecules in the lipidic cubic phase. This information was one of the important steps in breaking throw the 'dogmas' of the crystallization and new approaches to the crystallization of membrane proteins have been developed (Gordeliy, unpublished). These new methods have been applied for the first time for crystallization of the complex of two membrane proteins (sensory rhodopsin II (NpSRII receptor) and transducer NpHtrII from ***Natronobacterium pharaonis***) which transfers a signal from outside to inside of the bacterial cell (Gordeliy et al., 2002).

The X-ray structure of the complex between NpSRII and the receptor binding domain of NpHtrII has been solved at 1.94 Å resolution and provides an atomic picture of the first signal transduction step (Gordeliy et al., 2002) . The sensor activate a signal transduction chain similar to that of the two-component system of eubacterial chemotaxis. The link between the photoreceptor and the following cytoplasmic signal cascade is formed by the transducer molecule which tightly and specifically binds to its cognate receptor by means of its two transmembrane helices (TM1; TM2) (Fig. 2).

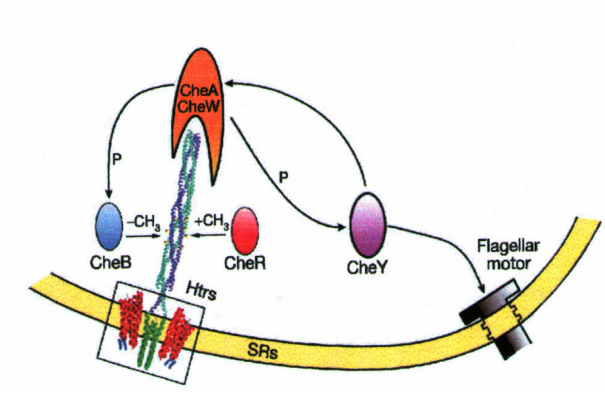

Fig.2. Fold of the receptor/transducer complex a, Top view from the cytoplasmic side: ribbon diagram with α-helices in red for the receptor and green for the transducer, β-strands in blue, and coils in gray. The labels of the symmetry related complex are marked by an apostrophe. The crystallographic symmetry axis is located between TM1-TM2 and TM1'-TM2'. b, Side view: by B-factor mobility coloring of the structures from light red/green (less mobile) to dark red/green (mobile). ES: extracellular side; CS: cytoplasmic side.

This work breaks new ground in several ways and is considered as a major advance in molecular cell biology of interections between proteins in a membrane embedded signal complex (Spudich, 2002). For the first time it gives the evidence for a common mechanism for signal transduction in phototaxis and chemotaxis.

References:

1. Bobarykina, G.[b, c] R. Efremov,[a, d] A. Islamov,[b] A. Kuklin,[b] L. Yaguzhinsky,[c] G. Fragneto-Cusani,[e] G. Bueldt[a] and V. Gordeliy[a, b, d]* (2002) SANS investigations of a lipidic cubic phase behaviour in course of bacteriorhodopsin crystallization. Submitted
2. Gordeliy, V.I., Labahn, J., Moukhametzianov, R., Efremov, R., Granzin, J., Schlezinger, R., Bueldt, G., Savopol, T., Scheidig A.J., Klare, J.P.& Engelhard M. (2002) Nature, 419, 484-487.
3. Gordeliy V.I., R. Schlesinger, R. Efremov, G. Bueldt, J. Herbele (2002) "Crystallization in lipidic cubic phase: A case study with bacteriorhodopsin" : in the book "Membrane Protein Protocols : Expression, Purification and Crystallization " (THE HUMANIA PRESS INC. USA).(A review) In press.
4. Landau, E.M. & Rosenbush, J.P. (1996). Proc. Natl. Acad. Sci. USA 93, 14532-14535.
5. Nollert, P., Qui, H., Caffrey, M., Rosenbush, J. & Landau, E. (2001). FEBS Letters 504, 178-186.
6. Pebay-Peyroula, E., Rummel, G., Landau, E.M., & Rosenbush J.P. (1997). Science 277, 1677-1680.
7. Spudich, J. (2002) Spotlight on receptor/transducer interection. Nature Str. Biol. 9 (11), 797-799.

SAXS STUDY OF TREHALOSE INFLUENCE ON THE DMPC VESICLE STRUCTURE

M.A.Kiselev[1], I.V.Gapienko[1], J.Perez[2], C.Bourgaux[2]

[1]FLNP, JINR, Dubna, Russia
[2] LURE, Orsay, France

Introduction

The spatial resolution of small-angle scattering experiment mainly depends on the possibility to collect a scattering curve in the wide range of scattering vector with good enough resolution of scattering vector. Small-angle neutron (SANS) and X-ray (SAXS) scattering can be applied to study vesicles with diameter from 300 Å to 1000 Å in highly diluted systems. First efforts to investigate the internal membrane structure of unilamellar vesicles via SANS gave about 1.5 Å accuracy of the membrane thickness determination, accuracy of 2 Å of the hydrophobic core determination, and new information about membrane hydration [1]. A principal disadvantage of the SANS experiment is the incoherent scattering from hydrogen nuclei. 1% of lipid creates a background about $5 \cdot 10^{-3}$ cm^{-1}, which limited the maximum value of the scattering vector by 0.3 Å^{-1} [1]. This limitation does not exist for SAXS. An important problem to be solved is to enhance the contrast due to the weak X-ray contrast between phospholipid bilayer and water [2]. The X-ray contrast between DMPC molecules and water is $|\Delta\rho_x| = 0.14 \cdot 10^{10}$ cm^{-2}. In the case of neutron scattering, the contrast is $|\Delta\rho_n| = 0.45 \cdot 10^{10}$ cm^{-2}, whereas the application of D_2O increases the neutron contrast to $|\Delta\rho_n| = 6.34 \cdot 10^{10}$ cm^{-2} [3]. 40% w/w sucrose increases the X-ray contrast by a factor of 10 compared to that of pure H_2O [2,3]. The purpose of present experiment is to carried out the investigation of trehalose and sucrose influence on the structure of DMPC vesicles via precise measurements of SAXS curve in the wide range of scattering vector.

Sample preparation and methods

20%, 30% and 40% (w/w) aqueous trehalose and sucrose solutions were used. DMPC concentrations were equal to 1% and 3% (w/w). Unilamellar DMPC vesicles were prepared via extrusion technique. SAXS spectra were collected at D24 spectrometer of DCI synchrotron ring of LURE, Orsay, France. Sample temperatures during were fixed at 10^0C and 30^0C. Sample to detector distances were equal to 875 mm, and 2883 mm., which allowed to collect spectra in the range of scattering vectors values from 0.006Å^{-1} to 0.6Å^{-1}. The partway of photons was everywhere in the vacuum due to the application of sample holder with quartz capillary in the vacuum. This technique decreases the value of instrument background, that is important for the measurements of SAXS curve at large q range.

Results and discussions

Figure 1 demonstrates SAXS spectra from DMPC vesicles in 40% trehalose solution at temperatures 10^0C and 30^0C. Recorded SAXS curves are sufficiently different from the SANS curves obtained for the similar samples [1].

Three peculiarities relative to SANS can be mentioned from these curves without detailed model analyses:

1. Well recorded oscillations in the end of curve at large values of scattering vector, which correspond to the form factor of lipid bilayer. It is result of about 3% resolution in scattering vector of D24 instrument for q>0.2 Å^{-1}.
2. Maximum value of scattering vector recorded above the value of background is 0.4 Å^{-1} due to the low background from instrument and sample.

3. A different contrast variation between solution and membrane in neutron and X-ray experiment. This difference comes from differences in scattering length densities of lipid for X-ray and neutrons. In case of neutrons average scattering length densities of head group and hydrocarbon tails are approximately the same and strongly differ from average scattering length density of D_2O. At neutron scattering curves one can see minimum of intensity at value of q about 0.17 Å, which corresponds to scattering from lipid bilayer. Position of this minimum q_{min} can give us bilayer thickness that is equal to $2\pi/q_{min} \approx 37$ Å [5]. In case of X-ray scattering, average electron density of lipid is approximately the same as average electron density of solvent (H_2O). But electron density of head group and hydrocarbon tails are consequently above and below that is for water. Trehalose (sucrose) increases electron density of solvent. In this case, main part of contrast is originated from the electron density difference between hydrocarbon tails and solution.

Scattering intensity from the sample under investigation (see Fig.1) has minimum at q_{min} = 0.3 $Å^{-1}$ for T = 30^0C, and at q_{min} = 0.26 $Å^{-1}$ for T = 10^0C. It describes the deviation of hydrocarbon tail length from approximately 21 Å at 30^0C to 24 Å at 10^0C. This difference describes well-known hydrocarbon chain melting at the main phase transition temperature $T_m = 23^0$C.

Figure 2 demonstrate SAXS curves from DMPC vesicles in the 40% trehalose and 40% sucrose aqueous solutions. These curves are approximately the same. We can conclude for very diluted vesicular population that the influence of trehalose on membrane structure is the same as the influence of sucrose.

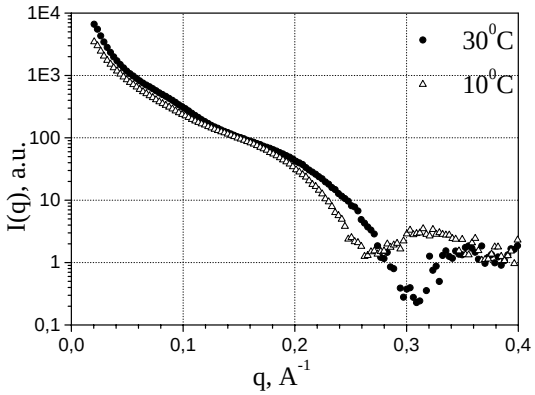

Fig.1. SAXS curves from 500Å DMPC vesicles in 40% trehalose solution at 10^0C and 30^0C

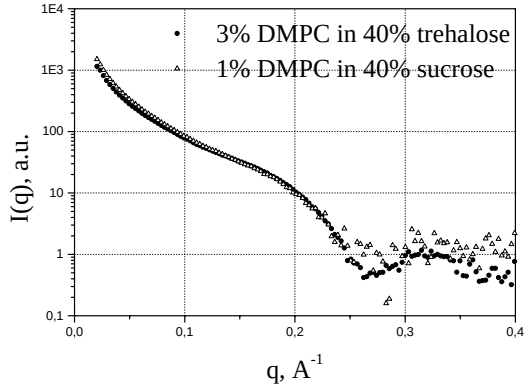

Fig.2. SAXS curves from 500Å DMPC vesicles in 40% trehalose solution and in 40% sucrose solution at 10^0C.

Conclusions

The recorded scattering curve is good enough to be analyzed via methods developed for SANS, but with better special resolution due to large q range recoded at D24 line [4,5]. This work is in progress now. The complementary application of SANS and SAXS technique for the investigation of vesicle structure can give more detailed and precise information about internal membrane structure due to the different contrast for neutron and X-ray.

This study was supported by the Ministry of Industry, Science and Technologies of Russian Federation (contract N№40.012.1.1.1148) and grand for Leading Scientific School.

References

1. H. Schmiedel, P. Joerchel, M.Kiselev, G. Klose.. J. Phys. Chem. B, 105 (2001) 111-117.
2. M.A. Kiselev, P. Lesieur, A.M. Kisselev, D. Lombardo, M. Killany, S. Lesieur, M. Ollivon. Nuclr. Inst&Method A 470 (2001) 409-416.
3. M.A. Kiselev, S. Wartewig, M. Janich, P. Lesieur, A.M. Kiselev, M. Ollivon, R. Neubert. Chemistry and Physics of Lipids (2002) in press.
4. M.A. Kiselev, P. Lesieur, A.M. Kisselev, D. Lombardo, V.L. Aksenov. J. Applied Physics A (2002) in press.
5. E.V. Zemlyanaya, M.A. Kiselev. JINR preprint P3-2002-163 (2002).

INVESTIGATION OF STRUCTURE OF ELONGATION FACTOR eEF-1A OF RABBIT LIVER BY NEUTRON SCATTERING AND MICROCALORIMETRY

I. Serdyuk[1,3], T. Budkevich[2], A. Timchenko[1], E. Tiktopulo[1], A. El'skaya[2], B. Negrutskii[2], V. Shalak[2], Z. Petrushenko[2], V. Aksenov[3], R. Willumeit[4], I. Kohlbrecher[5]

[1]*Institute of Protein Research, RAS, Pushchino, Russia*
[2]*Institute of Molecular Biology and Genetics, Kiev, Ukraine*
[3]*Frank Laboratory of Neutron Physics, JINR, Dubna, Russia*
[4]*Center for Neutron Research, Geesthacht, Germany*
[5]*Paul Scherrer Institut, Villingen, Switzerland*

It is well known, that most biological functions in a cell are performed by proteins, which have a rigid three-dimensional structure. Among these proteins one can find those having locally disordered regions, which are well detected by the X-ray structure analysis and nuclear magnetic resonance. For some of these proteins a connection between the structure of disordered regions and their function was determined.

In addition, there are proteins with globally disordered structure, having a definite function. Among them are small proteins of monomeric glucagon type and proteins performing regulatory functions. Moreover, at present there is a hypothesis that practically all regulatory proteins have a globally disordered structure. The most appropriate methods to investigate the structure of such proteins are small angle neutron scattering and microcalorimetry, which give the most comprehensive description of their structure. The application of these methods to investigation of the elongation factor protein of rabbit liver (eEF-1A) gives us ground to conclude, that the investigated protein is globally unstructured and has an unfolded conformation in solution. The very structure makes it possible for one protein to interact with different ligands. We presume, that the very absence of rigid-fixed conformation in factor eEF-1A can account for its well-known ability to form complexes with different cell ligands, starting from actin and tubulin to components of the ubiquitin-dependent proteolytic system.

Main experimental results

Conformation of the eukaryotic elongation factor extracted from rabbit liver was studied in solution by neutron scattering and scanning microcalorimetry. It was shown, that in contrast to its bacterial analogue (EF-1A), protein eEF-1A has no fixed, rigid structure in a wide range of guanidinediphosphate (GDP) concentrations. Its dimensions in solution surpass considerably those of EF-1A. Calculated from the heat absorption curves, the value of enthalpy for eEF-1A proved to be essentially lower than that of its prokaryotic analogue EF-1A, which is indicative of partially unfolded state of the molecule. Despite the absence of rigid structure in solution, eukaryotic elongation factor eEF-1A forms a solid complex with natural ligand (t-RNA), whose stability is 10^4 times higher than that of its prokaryotic analogue. In complex with t-RNA protein eEF-1A becomes essentially more compact.

Conclusions

The obtained experimental data make it possible to look in a principally new way upon some aspects of RNA-protein interactions in the process of protein biosynthesis in eukaryotic cells. Let us mention some of them.

1. Eukaryotic factor eEF-1A has a considerably more unfolded conformation in solution than its prokaryotic analogue EF-1A

Unlike its bacterial analogue EF-1A, protein eEF-1A extracted from rabbit liver has no fixed rigid structure in a wide range of GDP. Its dimensions in solution surpass considerably those of

EF-1A and depend essentially on GDP concentration. According to scanning microcalorimetry data, protein eEF-1A without GDP consists of two independent thermodynamic domains with transition temperatures 38 ^{o}C and 45 ^{o}C. In the presence of 20 мkM of GDP the second domain stabilizes: its transition temperature increases on 4 ^{o}C. The further increase of GDP concentration leads to a greater stabilization of the protein molecule: at 20 мM of GDP the protein melts as a single peak at the transition temperature 60 ^{o}C. Similar behavior is common for certain proteins: serum albumin, histons, some ribosomal proteins. Now it is known, that these proteins are not so compact as small globular proteins. Thus, for instance, only central part of a histon molecule is compact. According to calorimetric data, we come to the conclusion that protein EF1-A has no rigid fixed structure in the experimental conditions.

2. Conformational changes in eukaryotic factor eEF-1A during the forming of complex with tRNA are of much larger scale than those of prokaryotic factor EF-1A during a similar complex formation.

Despite the absence of fixed rigid structure in solution, eukaryotic elongation factor eEF-1A forms a solid complex with deacylated tRNA, the stability of which is 10^4 times higher than that of its prokaryotic analogue. The preliminary data indicate, that protein eEF-1A becomes considerably more compact in complex with tRNA, complex appears to be one molecule of tRNA per two molecules of the protein. Our data lead to a clear conclusion, that conformational changes in factor eEF-1A occurring during a complex formation are of much larger scale than those occurring during a complex formation between EF-1A and t-RNA in prokaryotic cell. As far as we know, such large conformational changes in proteins have not been described in literature until now.

3. Principles of functioning of the elongation factors in prokaryotic and eukaryotic systems are probably different.

Our experimental data point at principle differences of structural bases in functioning of the elongation factors in prokaryotic and eukaryotic cells. In solution prokaryotic factor EF-1A with a high affinity to tRNA has a folded compact conformation, which changes little interacting with tRNA. On the contrary, in solution eukaryotic factor eEF1-A has an unfolded non-fixed conformation, which compactifies greatly during increasing of GDP concentration and during interacting with tRNA. This gives us reason to presume that main idea based on the coincidence of principles of functioning in elongation factors in prokaryotic and eukaryotic systems must be essentially refined.

As a conclusion, it should be noted, that our new data demonstrate a fundamental importance of structural information obtained by small angle neutron scattering in the study of structure of globally unstructured proteins in solution and their interactions with natural ligands.

The paper is accepted for publication in the international scientific magazine “Biochemistry” under the title of “Conformation of the mammalian translation elongation factor 1A in solution”

SMALL-ANGLE NEUTRON SCATTERING STUDY OF THE BILAYER THICKNESS IN UNILAMELLAR DOPC LIPOSOMES PREPARED BY THE CHOLATE DILUTION METHOD: *N*-DECANE EFFECT

Daniela Uhríková[1], Norbert Kučerka[1], Akhmed Islamov[2], Alexander Kuklin[2], Pavol Balgavý[1]

[1]*Faculty of Pharmacy, J. A. Comenius University, Bratislava, Slovakia*
[2]*Frank Laboratory of Neutron Physics, Joint Institute for Nuclear Research, Dubna, Russia*

It has been observed that *n*-decane (C10) and its brominated analogs modulate the activity of sarcoplasmic reticulum Ca-Mg-ATPase reconstituted in unilamellar 1,2-diacylphosphatidylcholine liposomes by the cholate dilution method [1, 2]. Since the enzyme activity critically depends on the phosphatidylcholine acyl chain length [1-3], effects of *n*-alkanes on its activity have been ascribed to their effects on the thickness of lipid bilayer surrounding the protein [1]. The results of x-ray diffraction on the lamellar L_α phosphatidylcholine phase supported this conclusion – ~10 Å increase of bilayer thickness was observed in the presence of excess C10 [4]. We study the effect of C10 in unilamellar liposomes prepared by a cholate dilution method mimicking closely the enzyme reconstitution procedure.

Equimolar dioleoylphosphatidylcholine (DOPC) and sodium cholate in mixed micelles in D_2O were diluted step-wise to 8 mM DOPC concentration in D_2O. To the liposomes thus prepared, C10 was added in methanol. After methanol evaporation, the samples were studied by SANS. From the Kratky-Porod plot $\ln[I(Q)Q^2]$ vs. Q^2 of SANS intensity $I(Q)$ in the range of scattering vector Q values corresponding to 0.001 Å^{-2}≤Q^2≤0.006 Å^{-2}, the bilayer radius of gyration R_g and the bilayer thickness parameter d_g=12$^{0.5}$$R_g$ were obtained. The values of d_g indicate that the bilayer thickness is within the experimental error constant up to C10:DOPC~0.6 molar ratio, and increases then by 2.4±0.9 Å up to C10:DOPC=1.6 molar ratio (see Fig.).

The change of the DOPC bilayer thickness in unilamellar liposomes is relatively small up to *n*-decane:DOPC=1.6:1 molar ratio comparing to ~10 Å increase in the lamellar L_α phase. This seems to be caused by a change in the *n*-decane location when the bilayer becomes curved as in liposomes. The method of preparation and the full hydration of phospholipis in liposomes make this system to be a more appropriate model of bilayer surrounding the protein than the partially hydrated L_α phase. It is thus evident, that changes in Ca-Mg-ATPase activity induced by *n*-decane are not primarily caused by the changes in the bilayer thickness as originally proposed by Johansson et al. [1], but rather by the direct interaction of *n*-decane with the Ca-Mg-ATPase hydrophobic binding sites as suggested in [2, 3].

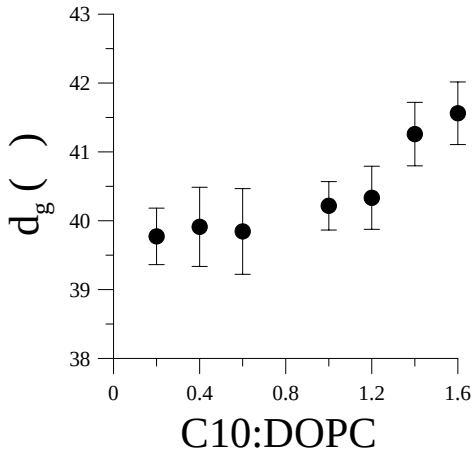

Acknowledgements
This study was supported within VEGA 1/7704/2000 and JINR 07-4-1031-99/03 projects. DU, NK and PB thank FLNP for hospitality.

References

1. A.Johannsson, C.A.Keightley, G.A.Smith, C.D.Richards, T.R.Hesketh, J.C.Metcalfe, J.Biol. Chem. 256 (1981) 1643-1650.
2. A.G.Lee, J.M.East, P.Balgavý, Pesticide Sci. 32 (1991) 317-327.
3. D.Uhríková, P.Balgavý, N.Kučerka, A.Islamov, V.Gordeliy, A.Kuklin, Biophys. Chem. 88 (2000) 165-170.
4. T.J.McIntosh, S.A.Simon. R. C. MacDonald, Biochim. Biophys. Acta 597 (1980) 445-463.

SELF-ASSEMBLY OF POLYELECTROLYTE RODS IN POLYMER GEL AND IN SOLUTION: SMALL-ANGLE NEUTRON SCATTERING STUDY

Yu.D.Zaroslov[1], V.I.Gordeliy[2], A.I.Kuklin[1], A.H.Islamov[1], O.E.Philippova[1], A.R.Khokhlov[1], G. Wegner[3]

[1]*Physics Department, Moscow State University, Moscow, Russia*
[2]*Laboratory of Neutron Physics, Joint Institute for Nuclear Research, Dubna, Russia*
[3]*Max-Planck-Institute for Polymer Research, Mainz, Germany*

Rigid-rod polyelectrolytes based on sulfonated poly-(p-phenylene) are able to aggregate in aqueous media due to the hydrophobic character of their backbone. This aggregation does not lead to precipitation because the charged sulfonate groups ensure the solubility of the aggregates in water. The first data on self-aggregation of sulfonated poly(p-phenylene)s in aqueous solutions were obtained by SAXS.[2] SAXS data showed that aggregated polymer chains take the form of columnar micelles, in which the phenylene backbones are oriented parallel to the axis of the micelle.[2] The magnitude of the radial aggregation number of the micelles was estimated for a series of sulfonated poly(p-phenylene) samples differing in charge density and in hydrophobicity. No information was obtained about the length of these aggregates from the evaluation of the SAXS data. It was emphasized [2] that the observed behavior of these polymers in solutions resembles the formation of supermolecular structures of some biogenic wormlike or stiff polyelectrolytes such as DNA or collagen. Therefore, a detailed study of the aggregates of rods in water could lead to better understanding of the processes of self-organization of biological macromolecules as well. On the other hand, it was shown that the ability of the macromolecules to aggregate can be used to immobilize them inside a water-swollen gel without formation of covalent bonds with the network.[3] The incorporation of rodlike polyelectrolyte in superabsor-bent hydrogels was proposed as a simple and efficient way for the improvement of mechanical properties of hydrogels in the swollen state which could be important for practical applications.[3] To control the properties of the gels with embedded rigid rods, the self-assembly of rod macromolecules inside the network should be studied. In our previous communication,[3] an indirect evidence of the self-aggregation of rods inside the gel was obtained from the results of the experiments on the swelling behavior of the gels. The aim of this work is to investigate the self-assembly of rigid-rod polyelectrolyte inside the water-swollen gel and to establish effects of the gel on the self-assembly of rods as well as of the rods on the gel structure.

Experimental Section

The synthesis of poly(sodium p-phenylene-sulfonate) PPP2 is described elsewhere.[3,4] Characterization of the precursor polymer which had sulfonate groups protected as 3,5-di-*tert*-butylphenolate is presented in refs 3 and 4. The degree of polymerization Pn of the precursor polymer is equal to 23.5; the contour length equals 18 nm. The persistence length of the precursor polymer was shown to be equal to 13 nm. This value can be regarded as the lower bound of the persistence length of the polyelectrolyte under study. Therefore, the PPP2 chains can be considered as rodlike chains. Polymer solutions were prepared by weighing the polymer and the solvent (D2O), mixing them and stirring at a temperature not higher than 95 °C for 20 min. For preparation of the polyacrylamide (PAAm) gels with embedded PPP2 rods, the mixture of D2O and H2O (80/20 v/v) of given composition was used as a solvent. The D2O/H2O mixture was added to 90 mg of acrylamide and to a calculated amount of PPP2 to have a resulting mass of the sample of 850 mg. Then 50 mg of 0.126 mol/L *N,N*-methylenebis(acrylamide) solution prepared in the same solvent was added, and the mixture was stirred at room temperature during at least 12 h. After the mixture was stirred, 50 mg of solution of ammonium peroxodisulfate (4.4×10^{-4} mol/L) and 50 mg of a solution of *N,N,N′,N′*-tetramethylethylenediamine (4.4×10^{-4} mol/L) prepared in

the same D2O/H2O mixture were added. The mixture was stirred again for 5 min and poured into special dismountable cell for further polymerization, which was performed over at least 24 h. D2O (99.9%) from Fluka was used as received. Water was purified with a Milli-Q system (Millipore).

Conclusions

Self-aggregation of rigid-rod poly(sodium p-phenylenesulfonate) in aqueous solution and inside water-swollen polyacrylamide gel was studied by small-angle neutron scattering. It was shown that both inside the hydrogel and in solution polyelectrolyte rods self-assemble into cylindrical aggregates having eight to nine single polymer chains in the cross-section, the chains being aligned parallel to the axis of the aggregate. The length of these aggregates is much higher than the contour length of a single chain. Gels with embedded rods were studied by contrast variation method in order to examine separately the scattering by the gel and by the rods. Two important observations were made. First, it was shown that the ordering of the rods in the gel resembles that in solution. Second, it was shown that the gel itself is more homogeneous in the presence of rods. Most probably, this effect is due to mobile counterions of rods, which counteract the formation of spatial inhomogeneities in the network during synthesis, because in an inhomogeneous network mobile counterions should be also distributed nonuniformly that is associated with significant translational entropy losses.

A comparative study of the aggregation of polyelectrolyte rods inside a water-swollen gel and in aqueous solutions was performed by SANS. It was shown that both in solution and in the gel the polyelectrolyte rods form cylindrical aggregates consisting of ca. 9 single molecules per a cross section. It was demonstrated that the polyelectrolyte rods affect the structure of PAAm network making it more homogeneous.

Acknowledgment

This research was supported by RFBR Grant No. 02-03-33259 and INTAS Grant No.00-445.

References

1. Yu.D.Zaroslov, V.I.Gordeliy, A.I.Kuklin, A.H.Islamov, O.E.Philippova, A.R.Khokhlov and G.Wegner Self-Assembly of Polyelectrolyte Rods in Polymer Gel and in Solution: Small-Angle Neutron Scattering Study Macromolecules 2002, 35, 4466-4471
2. Rulkens, R.; Wegner, G.; Thurn-Albrecht, T. Langmuir 1999, 15, 4022-4025.
3. Philippova, O. E.; Rulkens, R.; Kovtunenko, B. I.; Abramchuk, S. S.; Khokhlov, A. R.; Wegner, G. Macromolecules 1998, 31, 1168-1179.

STRUCTURE AND POSSIBLE CLUSTER FORMATION IN LIQUID LEAD-POTASSIUM ALLOYS

N.M.Blagoveshchenskii[1], Yu.V.Lisichkin[2], V.A.Morozov[1], A.G.Novikov[1], V.V.Savostin[1], A.L.Shimkevich[3]

[1]State Scientific Center, Institute for Physics and Power Engineering, Obninsk, Russia
[2]Institute of Atomic Power Engineering, Obninsk, Russia
[3]Institute of Nuclear Reactors, Russian Scientific Center "Kurchatovsky Institute" Moscow, Russia

Abstract. The static structure factors $S(Q)$ for liquid lead and Pb-K alloys obtained by neutron diffraction are presented. The binary system was investigated for potassium concentrations of 5, 14, 22, and 25 at.% at 660 K and for the eutectic point of 9 at.% at 630 K. A weak elevation of $S(Q)$ is found in front of the main peak for the $Pb_{0.95}K_{0.05}$ and $Pb_{0.91}K_{0.09}$ alloys and a prepeak for the $Pb_{0.86}K_{0.14}$, $Pb_{0.78}K_{0.22}$, and $Pb_{0.75}K_{0.25}$ ones. This points to the formation of clusters for rising potassium concentration in liquid lead.

Alloys of lead and potassium were and remain untill now the subject of numerous macro- and microscopic investigations in a wide temperature range by neutron diffraction [1], molecular dynamics [2], and the reverse Monte Carlo method [3]. The increased interest to this systems results from Zintl clusters which possibly exist in the liquid Pb-K matrix for potassium concentration ? 25 at.% in the form of quasi-molecular group, $(Pb_4)^{4-}(K^+)_4$, in tetrahedral packing atoms. Our preliminary data for a liquid Pb-K alloy in eutectic point of 9 at.% K do not confirm such clusterisation. Therefore, close attention is needed to investigate the microstructure of the Pb-K melt for potassuim concentration ranging from 5 up to 25 at.%. The binary Pb-K system was also studied for possible correction of the properties of a lead melt as a prospective coolant for fast nuclear reactors.

These are the reasons which have induced us to carry out neutron-diffraction research of four Pb-K alloys at potassium concentrations of 5, 14, 22, and 25 at.%, as well as liquid lead for comparing with the binary system at 660 K, which is ? 15 K higher than the liquidus point for a Pb-K alloy of 25 at.% K. We also have carried out similar research of the eutectic alloy Pb-K (9 at.%) at 630 K.

1. Experimental

The DIN-2PI time-of-flight spectrometer [4] was used. It is located at one of the neutron beams of the IBR-2 pulsed reactor (Frank Laboratory of Neutron Physics, JINR, Dubna). The neutron momentum transfer, Q, of the diffraction experiments was in the range of $0.3 < Q < 22$ E^{-1}. The resolution, $?Q/Q$, was estimated at about 5%.

Samples of liquid metal are made as a cylindrical layer of 2 mm in thickness, 30 mm in outer diameter, and 110 mm in height. Each sample is cased in 0.15-mm thick vanadium foil to avoid coherent scattering from the container. Information for pure lead (99.99%) and Pb-K alloys was obtained in the same experimental conditions for directly comparing the data.

The measurement procedure and primary data processing were standard [5]. The background was subtracted from experimental spectra. The corrections on self-shielding the sample in the container, container, and the vanadium standard were entered; the effect of container scattering was taken into account. A special attention was given to the multiple scattering correction, which is very important in the case of the liquid lead [6]. A correction for inelastic neutron scattering was not made.

2. Results and discussion

Experimental plots of $S(Q)$ are shown in Fig. 1. The data for Pb-K (25 at.%) are close to known results [1]; however in this work an enhanced intensity of $S(Q)$ at the small-Q region was not found by us. For the main peak of $S(Q)$, its amplitude is decreased with growth of potassium concentration in the lead melt, the half-width grows, and the position is displaced towards small Q. As seen in Fig. 2, at potassium concentrations of 14, 22, and 25 at.%, a prepeak at Q ? 1 E^{-1} is obviously visible and can be assigned to the possible existence of the Zintl clusters in the Pb-K alloy [1].

The position of the first diffraction peak and a distance between scattering centers are connected by a ratio: $R_{max} = 7.73/Q_{max}$. Q_{max} ? 1.05 E^{-1} from our data and, hence, we have R_{max} = 7.4 E^{-1}. The prepeak area grows, and its half-width is decreased with the growth of the potassium concentration over the eutectic point. Both these circumstances testify that the clusterization of the Pb-K melt amplifies with growth of the K concentration.

At a concentration lower than the eutectic point, the prepeak disappears.

The differential structure factors obtained by subtraction of $S(Q)$ for lead from those for the Pb-K alloys are shown in Fig. 3. It is visible that the curves for potassium concentrations of 5, and 14 at.% differ in form from those for 22 and 25 at.%. This specifies a character of atomic structure correlation in the Pb-K melt at a potassium concentration > 14 at.%. In comparing differential curves for the main peak of $S(Q)$ and those for the prepeak, it appears that their amplitudes are changed equivalently with the growth of potassium concentration. Thus, the short order of Bernal's tetrahedral chains in liquid lead is deformed continuously and transformed into the clusters at a growing potassium concentration in the lead melt.

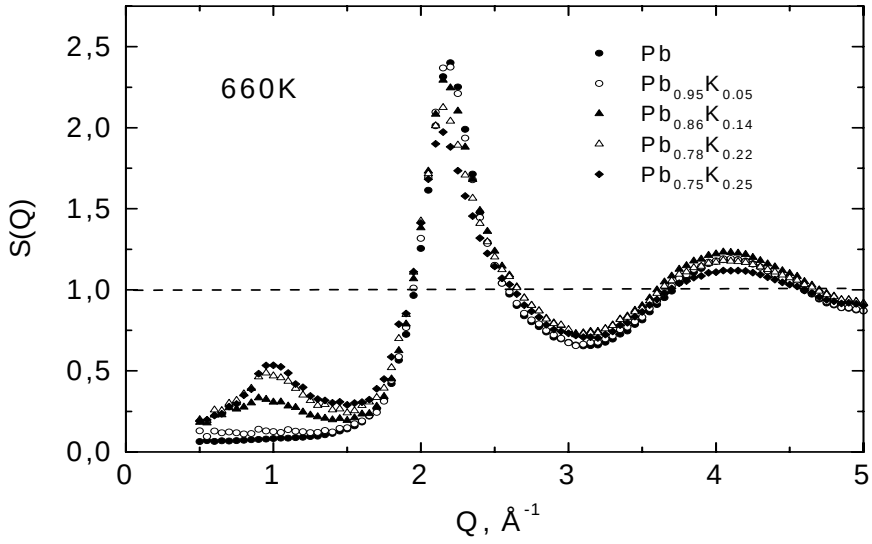

Fig. 1. The structure factors of liquid Pb and Pb-K alloys.

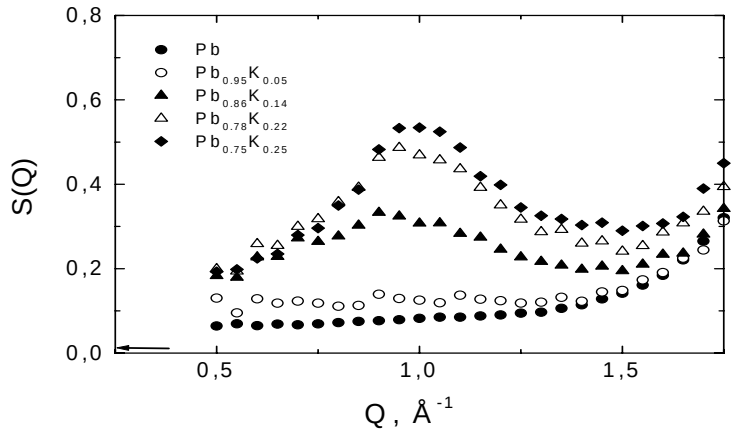

Fig. 2. The structure factors of liquid Pb and Pb-K alloys for a small-Q region. An arrow depicts the S(0) value in a hydrodynamic limit.

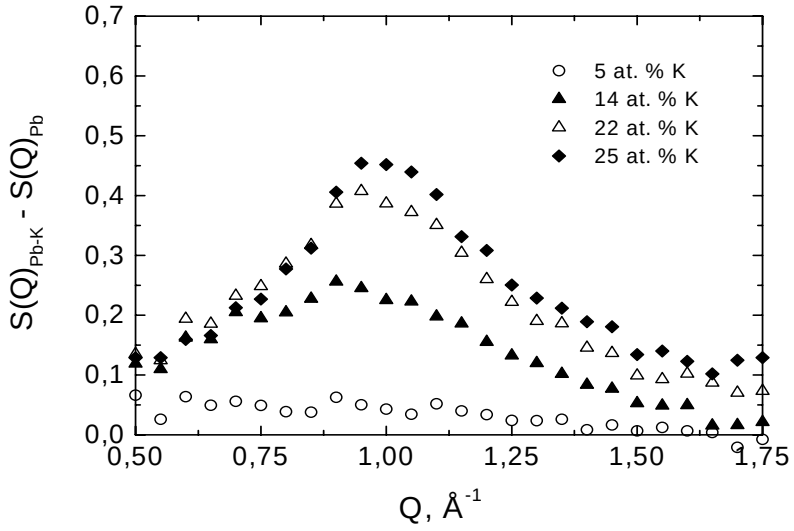

Fig. 3. The differential structure factors for Pb-K melts in the small-Q region.

Acknowledgements. This work was performed under financial support of the Russian Federation Programme 'Actual Investigation of Condensed Matter' under the Project 'Neutron Studies', and the Russian Foundation for Basic Research, Project No. 00-02-017563.

References

1. H.T.J. Reijers, W. van der Lugt, C. van Dijk, M-L. Saboungi, J. Phys.: Condens. Matter, 1989, v 1, p. 5229.
2. H.T.J. Reijers, W. van der Lugt, M-L. Saboungi, Phys. Rev. B, 1990, v. 42, p. 3395.
3. M.A. Howe, R.L. McGreevy, J. Phys.: Condens. Matter, 1991, v. 3, p. 577.
4. User Guide. Neutron Experimental Facilities for Condensed Ìatter Investigation at JINR. Ed. by V. Sikolenko. JINR Press, Dubna, 1997.
5. C.G. Windsor: Pulsed Neutron Scattering. Taylor and Francis Ltd, London, 1981.
6. D.M. North, J.E. Enderby, P.A. Egelstaff, J. Phys. C, 1968, v. 1, p. 784.

STRUCTURAL PHASE TRANSITIONS AND LATTICE DYNAMICS OF SOLID MESITYLENE

I. Natkaniec

Frank Laboratory of Neutron Physics,INR, Dubna, Rosja
H. Niewodniczański Institute of Nuclear Physics, Kraków, Poland

K. Hołderna-Natkaniec

Institute of Physics, A. Mickiewicz University, Poznań, Poland

Mesitylene or 1,3,5-trimethylbenzene - $C_6H_3(CH_3)_3$, is a well known organic solvent characterized by the relatively low freezing (227K) and high boiling (437K) temperatures. Because of high content of hydrogen and the assumed weakly hindered rotation of methyl groups in the solid phase, which can remove energy from neutrons, this compound has been recommended as neutron moderator [1], and used for construction of the TCNS cold neutrons source at the TRIGA Mark II pulsed reactor of the NETL in Austin [2]. However, the structure and dynamics of solid mesitylene until now is not well investigated.

The temperature dependence of the IINS spectra has confirmed the occurrence of rotational freedom of methyl groups in solid mesitylene at T=100K, but at T=20K the rotational jumps seems to be frozen [3]. The NDP spectra measured in this experiment for the lattice spacing up to 0.6 nm the do not indicate any diffraction peaks. As follows from the temperature dependence of the Raman spectra of $C_6H_3(CH_3)_3$, the frequencies of lattice modes and certain internal modes change at 95 and 195 K [4]. The DSC thermograms reported in [4] show two endothermic peaks for mesitylene in solid phase at 91 K and 188 K, and three endothermic peaks at 220, 222 and 227 K corresponding to the melting. This result was interpreted as manifestation of the presence of three different structural modifications Iα, Iβ and Iγ, in the high-temperature solid phase I.

Our recent simultaneous IINS and NPD investigations performed on the NERA spectrometer [5] at the IBR-2 pulsed reactor, shown up that solid mesitylen can exist in the different crystallographic structures depend on the cooling rate. At the cooling rate of 2K/min, overcooled liquid was freezing in the structure of phase II, and the first order structural phase transitions from phase II to phase III were detected at ~90 K for mesitylene-D3, and at ~100K for mesitylene-D9. Transition from phase II to phase I is not reversible, it start at approx. 190K but the NDP spectra shown pure phase I structure only after annealing of the samples at 220K. Phase I has the only one structural modification and at cooling come to be stable with respect to phases II and III. Phase II, in presence of the participation of phase I, can be also over-cooled to low temperatures [6].

Thus, three different solid phases of mesitylene can exist and may be investigated at the low temperatures. Here we present the results of the NPD and IINS investigations of solid mesitlene-D0, which were performed in order to check that solid phases obtained for partially deuterated samples can be observed as well in the hydrogenous substance [7].

The characteristic NPD spectra of the three solid phases of $C_6H_3(CH_3)_3$ recorded at T=20 K, are presented in Fig.1. The density of the phonon states and internal modes of the mesitylene molecule obtained in the range up to 300 cm^{-1}, on the basis of the IINS spectra for different phases of the crystalline mesitylene at T=20 K, are presented in Fig. 2. The intense bands at the frequencies 155 $cm^{-1}$and 190 cm^{-1} present in the spectrum of phase III, are interpreted as corresponding to librations of the methyl groups. These bands disappear in the spectra of phases II and I, which testifies to a significant decrease of the barrier for rotation of the CH_3 in these phases and a shift of the libration bands into the range of lattice vibrations, below 140 cm^{-1}. The spectrum $G(\omega)$ for the phase II in the range of the lattice vibrations is characterised by broadened phonon bands and the so-called boson peak typical of glass phases, which corresponds to a much greater density of vibrational states in the acoustic phonon range, below 50 cm^{-1}. The above evidence suggests that

phase II could be classified as the proton glass. The internal vibrations of the mesitylene molecule of frequencies above 200 cm^{-1} practically do not depend on the crystalline structure.

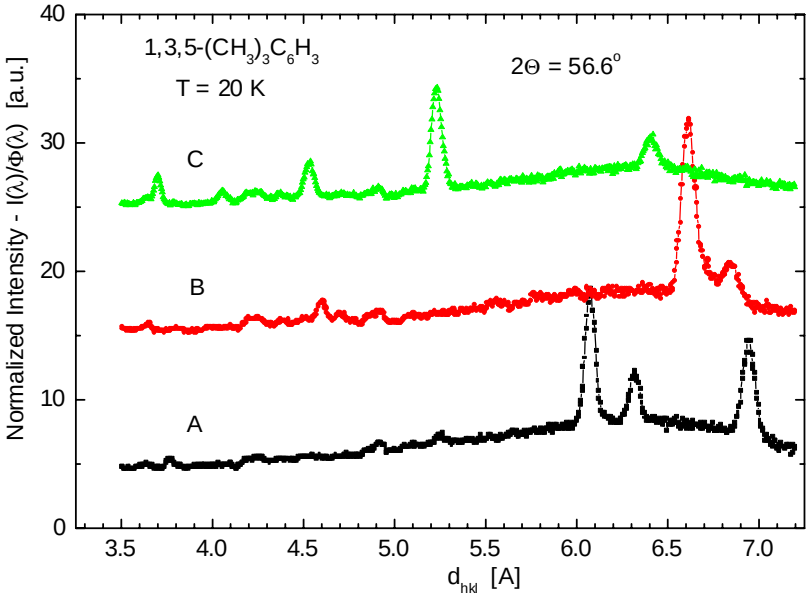

Fig. 1. Neutron diffraction spectra recorded for $C_6H_3(CH_3)_3$ at T=20 K, A – phase III, B – phase II, C – phase I.

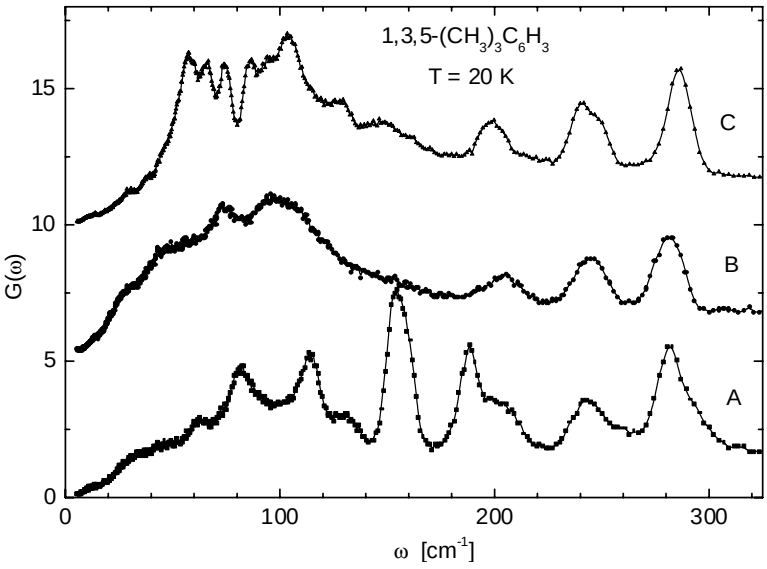

Fig. 2. The vibrational density of states for different phases of crystalline mesitylene: A – phase III, B – phase II, C – phase I.

References

1. M. Utsuro, M. Sugimoto, J. Nuc. Sci. Technol., 14(5) (1977) 390-392.
2. K. Unlu, C. Rios-Martinez, B.W. Wehring, J. Radioanal. Nucl. Chem., 193 (1995) 145-154.
3. L. Cser, K. Hołderna-Natkaniec, I. Natkaniec, A. Pawlukojc, Physica B, 276-278 (2000) 296-297.
4. M. Yamazaki, M. Tanaka, T. Inoue, Y. Suzuki, Y. Nibu, H. Shimada, R. Shimada, Bul. Chem. Soc, JPN., 73 (2000) 837-842.
5. Natkaniec, S.I. Bragin, J. Brankowski, J. Mayer, in Proceedings of ICANS XII Meeting, Abingdon 1993, RAL Report 94-025, (1994), Vol. I., p. 89-96.
6. Natkaniec, K. Hołderna-Natkaniec, American Conference on Neutron Scattering, Knoxville, Tennessee, June 22-27, 2002, p.98.
7. Natkaniec, K. Hołderna-Natkaniec, Proceedings of 6th Meeting of the Collaboration on Advanced Cold Moderators, Julich, 11 – 13 September 2002.

THE INVESTIGATION OF AMMONIUM ION DYNAMICS IN $K_{1-x}(NH_4)_xBr$ MIXED CRYSTALS

L.S.Smirnov [1,2], I.Natkaniec [1], V.Yu.Kazimirov [1], V.V.Dolbinina [3], L.A.Shuvalov [3]

[1] *I.M.Frank Laboratory of Neutron Physics, Dubna, Moscow region, Russia*
[2] *SSC RF Institute of Theoretical and Experimental Physics, Moscow, Russia*
[3] *A.V.Shubnikov Institute of Krystallografiya of RAS, Moscow, Russia*

The crystal structures of KBr and NH_4Br have different space groups at room temperature and form the $K_{1-x}(NH_4)_xBr$ solid solutions with limited regions near K and NH_4^+ [1]. KBr do not have phase transitions from room temperature to low but NH_4Br undergoes the series of phase transitions [2,3]:

α-phase ⇔ 410.8K ⇔ β-phase ⇔234.9K ⇔ γ-phase ⇔ (105-78) K ⇔ δ-phase.

The cubic disordered α-phase has sp. gr. $Fm3m\text{-}O_h^5$, the cubic disordered β-phase has sp. gr. $Pm3m\text{-}O_h^1$, the ordered tetragonal γ-phase – sp. gr. $P4/nmm\text{-}D_{4h}^7$ and ordered cubic δ-phase has sp. gr. $P\text{-}43m\text{-}T_d^1$. It is worth to note that until recent time the x-T phase diagram of the $K_{1-x}(NH_4)_xBr$ mixed crystals was studied seldom.

There are presented the results of ammonium dynamics study of $K_{1-x}(NH_4)_xBr$. These investigations were carried out by the neutron powder diffraction (NPD) and the inelastic incoherent neutron scattering (IINS) on the samples with ammonium concentrations x= 0.14, 0.24, 0.52, 0.83 and 1.0 at T=23 K. These powder samples were prepared from appropriate water solutions by slow evaporation. The NPD and IINS spectra were measured on the NERA-PR spectrometer.

Concentrations x of $K_{1-x}(NH_4)_xBr$ were determined by the intensities from translational ν_5 and librational ν_6 modes of the IINS spectra normalized on weights and expose times. The obtained NPD spectra from $K_{1-x}(NH_4)_xBr$ were used for the determination of lattice parameters of observed α- and β-phases. It was shown that samples with x=0.14 and 0.24 are α-phase and samples with x=0.52 and 0.83 contain α- and β-phases (Fig. 1a). The dependences of the lattice parameters for $K_{1-x}(NH_4)_xBr$, at room temperature from [1] and at 23 K from recent investigation, are presented in Fig. 1b.

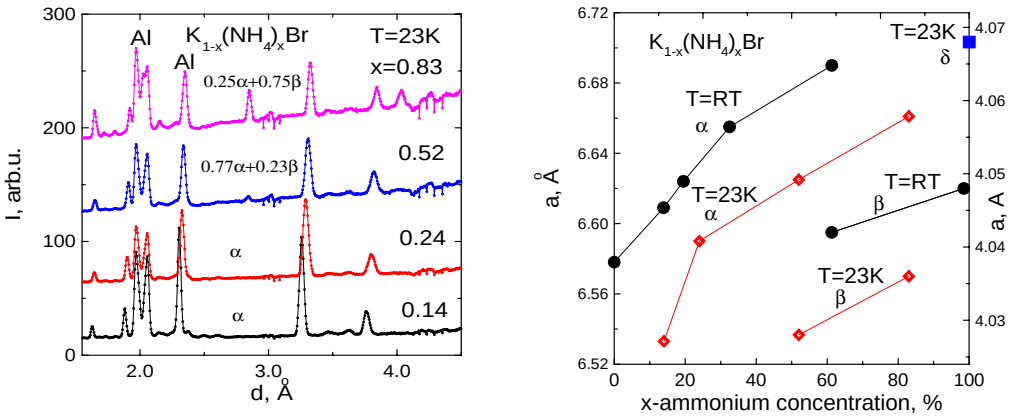

Fig. 1. (a)-the NPD spectra of $K_{1-x}(NH_4)_xBr$ at 23 K, (b)-concentration dependence of lattice parameters for $K_{1-x}(NH_4)_xBr$ (● - data at T=RT from [1], ◘ - recent results at T=23 K).

The obtained IINS and calculated G(E) spectra for $K_{1-x}(NH_4)_xBr$ are presented in Figs. 2(a) and 2(b) respectively. The IINS and G(E) spectra of samples with x=0.14 and 0.24 are suit to α-phase and that of samples with x=0.52 and 0.83 are suit to α- and β-phases.

The IINS spectra of the samples with x=0.14 and 0.24 show the contributions of the quasielastic incoherent neutron scattering (QINS) which is diminish with increasing of ammonium

concentration. Such behaviour can be explained as due to the orientational glass state. The G(E) spectra gives the possibility to determine the changes in $K_{1-x}(NH_4)_xBr$ with ammonium concentration. There are selected resonance modes E_r^1 and E_r^2, local translational mode ν_5 and librational mode ν_6 in α-phase (x=0.14 and 0.24) and only local translational mode ν_5 and librational mode ν_6 in β-phase (x=0.52 and 0.83). It is worth to note the splitting of librational mode ν_6 in β-phase on two sub-bands. Other interest peculiarity of the G(E) spectrum of $K_{0.17}(NH_4)_{0.83}Br$ is the appearance of $\nu_5+\nu_6$ Raman mode and $2\nu_6$ second harmonic in β-phase. The G(E) spectrum of NH_4Br at 23 K is suit to crystal structure of δ-phase. Concentration dependence of energies for observed modes in α- and β-phases of $K_{1-x}(NH_4)_xBr$ s presenter in Fig. 3.

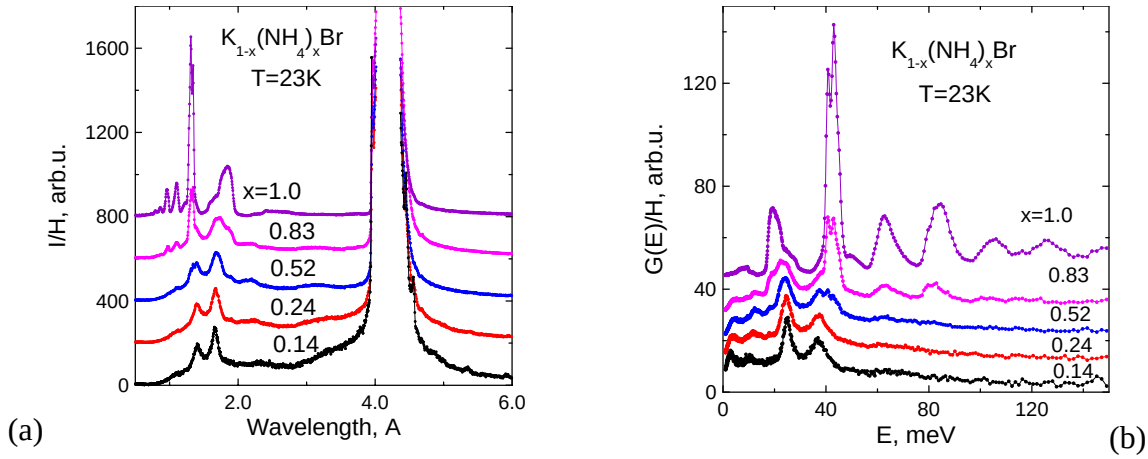

Fig. 2(a)-the IINS spectra of $K_{1-x}(NH_4)_xBr$ at 23 K, Fig.2(b)-the G(E) spectra of $K_{1-x}(NH_4)_xBr$ at 23 K.

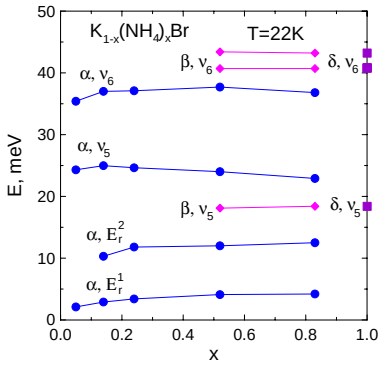

Fig. 3. The energies of modes in different phases of the $K_{1-x}(NH_4)_xBr$ mixed crystals.

Authors thank RFBR (grant № 02-02-17330) and L.A.Shuvalov's school (grant № 00-15-96797) for the partial financial support.

References:

1. R.Havighurst, E.Mack, Jr., F.C.Black, J.Am.Chem.Soc., 47 (1925) 29.
2. A.Levy, S.W.Peterson, J.Am.Chem.Soc., 75 (1953) 1536.
3. C.H.Perry, R.P.Lowndes, J.Chem.Phys., 51 (1969) 3648.

NEW COMPOSITE MATERIALS: MAGNETIC NANOPARTICLES IN COPOLYMER FILMS BY SPECULAR AND OFF-SPECULAR NEUTRON SCATTERING

V.Lauter-Pasyuk [1,2,3], H. J.Lauter[3], V.Aksenov[2], W.Petry[1], G.P.Gordeev[4], P.Müller-Buschbaum[1], B.P.Toperverg [4,5] , A.Petrenko[2]

[1]TU München, Lehrstuhl E13
, [2]JINR, Dubna
[3]ILL, Grenoble
[4]PNPI, Gatchina
[5]IFF Jülich

We performed the detailed studies of the new composite lamellar films with a high concentration of the nanoparticles. It is shown that the polystyrene - polymethylmethacrylate P(S-b-MMAd) copolymer multilayer orders the assembly of PS-coated Fe_3O_4 nanoparticles into a lamellar array along the PS layers of the host matrix. The application of neutron specular reflection and off-specular scattering accompanied by a two-dimensional data analysis allows for a detailed description of the nanoparticles distribution inside the copolymer matrix. As a result, the parameters of the transverse and the lateral structure for pure of the incorporated magnetite Fe_3O_4 nanoparticles with the average diameter of 10 nm were obtained.

Diblock-copolymers, dissolved in toluene, cast and spin-coated onto silicon substrate. Self-assembly of the copolymer matrix is determined by the non-miscibility of the two chemical components. The lamellae are parallel to the substrate and the surface of the film and their thickness is given by nL/2 with n integer even and L the lamellar period (PMMA-PS-PS-PMMA). By coating the nanoparticles with one or another type of the polymer chains (prior to the adding to a toluene solution of the copolymer) we provide a control on the nanoparticle distribution within one or another part of lamellar structure.

We succeeded to incorporate Fe_3O_4 nanoparticles with the average diameter of 10 nm up to 8% of the volume fraction. Even for a high concentration particles stay included in the film and the lamellar structure is not destroyed. Periodic location of the particles as well as the transverse and lateral structure of the lamellar pure copolymer and composite films was determined using neutron specular reflection and off-specular scattering.

The presence of the nanoparticles induces distortion of the copolymer matrix. The neutron off-specular scattering contains valuable information about the internal structure of the film, including the nanoparticles' distribution, lateral structure of the roughness and its conformity through the lamellar multilayer and also the surface structure of the film.

Earlier developed theoretical approach based on the Distorted Wave Born Approximation (DWBA) allows for a description of a full 2-dimensional intensity map, including the dynamical range close to the total reflection region [1, 2].

The experiments on neutron specular reflection and off-specular scattering were performed on the REMUR reflectometer, using the time-of-flight method with the wavelength band λ from 1 to 12 Å and the fixed scattering angle a = 0.014 rad. The data were recorded with a position sensitive detector in a wide range of incoming and outgoing wavevectors p_i and p_f. The reflected and scattered intensities are depicted in Figure as functions of $(p_i + p_f) = Q_z$ and $(p_i - p_f)$ for two samples without (a) and with (d) nanoparticles. The specular reflectivity runs along the line $p_i - p_f = 0$ and shows regular oscillations, which are determined by the total thickness of the film. The off-specular intensity in a form of the Yoneda scattering spreads out left and right from the specular intensity line indicating the presence of the surface and the substrate roughness.The multilayer structure formed by the lamellae oriented parallel to the film surface causes the appearance of the Bragg peaks on the reflectivity line. The presence of the Bragg peaks for the sample with incorporated nanoparticles (Figure d) proves that the multilayer structure persists and is not

destroyed by a rather high concentration of the nanoparticles. However, the positions of the Bragg peaks are shifted towards smaller values of Q_z, indicating the increase of the lamellar period due to the presence of the nanoparticles. The off-specular intensity crossing the specular line in the Bragg peak position (so called Bragg sheets [2-4]) is due to the interfacial roughness. This intensity appears when the roughness is correlated not only within each interface but also at different interfaces across the film. The degree of this conformity regulates the ratio between the intensity of the Bragg sheet and the Yoneda scattering. The off-specularly scattered intensity from the sample with nanoparticles does not change considerably, that proves a certain degree of conformity of the interfacial roughness.

The two – dimensional fit to the experimental data was performed using the model described in details earlier [1-4] and the results will be published elsewhere[5].

This work was supported by the BMBF (grant No 03DUOTU1/4) and NATO (Grant No. PST.CLG.976169).

References

1. Lauter-Pasyuk V, Lauter H.J., Toperverg B.P., Nikonov O., Petrenko A., Schubert D., Petry W., Aksenov V. ILL Millennium Symposyum 2001, 59, http://www.ill.fr/pages/menu_g/docs/ILL_Proceedings.pdf
2. Lauter-Pasyuk V, Lauter H.J., Toperverg B.P., Nikonov O., Petrenko A., Schubert D., Schreiber J., Burcin M., Petry W., Aksenov V. Appl. Phys. A 2002, 74
3. Toperverg B.P., Lauter-Pasyuk V, Lauter H.J., Nikonov O., Ausserre D., Gallot Y. Physica B 2000, 276-278, 355
4. Toperverg B.P., Lauter-Pasyuk V, Lauter H.J., Nikonov O., Ausserre D., Gallot Y. Physica B 2000, 283, 60
5. Lauter-Pasyuk V, Lauter H.J., G. Gordeev, P.Müller-Buschbaum, Toperverg B.P., M., A. Petrenko, Jernenkov, V. Aksenov, Petry W., to be published

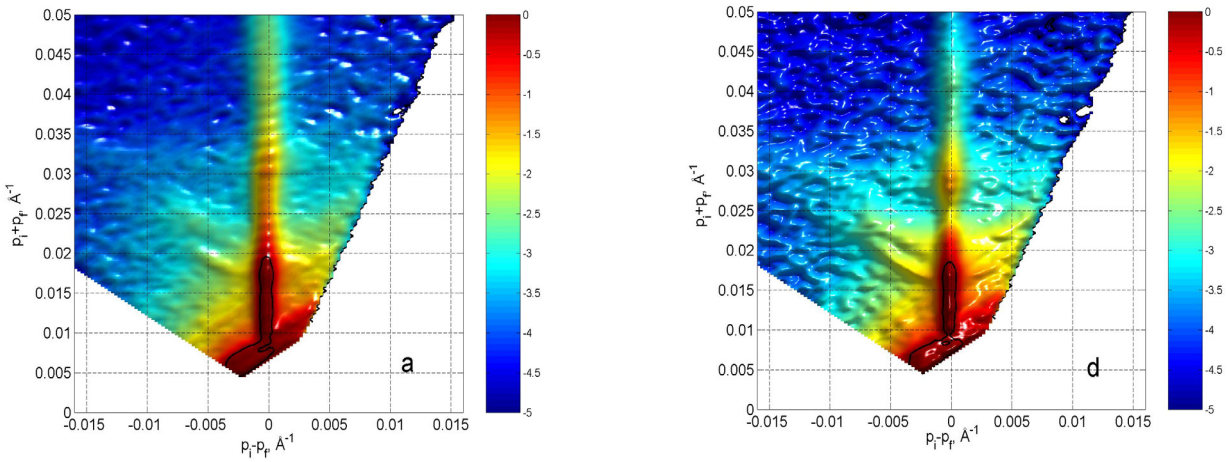

Figure. Experimental 2-dimensional intensity map from annealed samples of pure P(S-b-MMAd) thin film (a) and similar copolymer film with incorporated Fe_3O_4 nanoparticles (d); p_i and p_f are the perpendicular to the surface components of the incoming and outgoing neutron wave vectors, respectively. The strong intensity along the line (p_i - p_f) = 0 corresponds to the specular reflection, the Yoneda scattering intensity spreads left and right from the specular line.

EXPERIMENTAL OBSERVATION OF THE UCN FOCUSING IN TIME

A.I.Frank, G.V.Kulin, A.N.Strepetov[1], P.Geltenbort[2]

[1] *Russian Research Center "Kurchatov Institute", Moscow, Russia*
[2] *Institute Laue Langevin, Grenoble, France.*

In the recent paper [1] the attention was drawn to the circumstances that by the action at a neutron wave with any nonstationary device it is possible to change neutron velocity in such a way, that conditions of neutron focusing in time would be satisfactory. In particular, the possibility of using the effect of neutron energy quantization at neutron diffraction by the moving grating for the construction of "time lens" was discussed. Recently this effect was observed experimentally [3,4]. Concluding the paper [4] we wrote: "The idea of neutron time-focusing, as proposed in [1], now looks more realistic". At the moment we can report about the first experimental observation of the neutron time focusing using nonstationary action at the neutron wave.

Figure 1 illustrates the idea of the experiment. Let monochromatic neutrons be moving along the X axis. A device, time lens, capable of changing the neutron energy follows the defined $\Delta E(t)$ dependence, which is positioned at the point x=a. As a result, the neutrons, which leave the source during some period T, reach the point of observation located at L simultaneously.

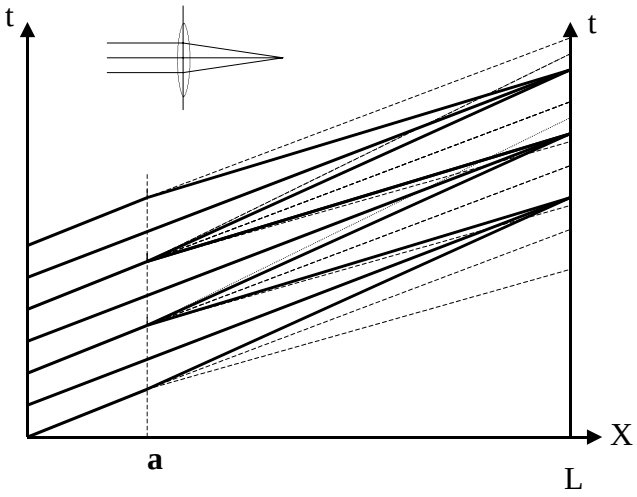

Fig .1. The time – space diagram of the experiment

In our experiment the active action at the neutron energy was due to diffraction of the rotating grating. The experimental set up, the modified spectrometer [5], was used in the time-of-flight mode. The neutron interference filter (NIF) was used for the monochromatization of ultracold neutrons (UCN). Only the UCNs with a narrow spectrum of vertical velocities i.e., a maximum of 4.52 m/s and FWHM of about 0.085 m/s, passed through the monochromator and reached the grating just below it. Using a motor, the grating could be spinned about the vertical axis at 6000 rpm. The vertical neutron guide with glass mirror walls transported the UCN to the neutron thin-layer scintillation detector. The (n,α) reaction at the Li^6 isotope was used for the conversion of neutrons to the charged particles. The monochromator – detector distance, i.e. the flight path, was 70 cm.

The grating was manufactured on the surface of a silicon disk, 150 mm in diameter and 0.6 mm thick. radial grooves were made by the lithographic technique in its peripheral region. The depth of grooves was 0.14 microns, which corresponded to the phase shift of π at neutron refraction in silicon. The distance α between the grooves was a function of the azimuth at the grating surface. When the grating was spinning, UCNs passed through the part of it with the space period α and the space frequency α^{-1}, respectively. As a result, the transmitted waves were modulated with the frequency $\boldsymbol{\Omega = 2\pi V\alpha^{-1}}$, where V is the grating linear velocity (see fig.3). So the modulation frequency Ω was variable at the constant spinning frequency.

After passing the grating, which acted as a phase modulator, the transmitted state was the nonstationary superposition of waves, each of which had the energy of $\hbar\boldsymbol{\omega_n}$ and corresponded to the wave number $\mathbf{k_n}$

$$\Psi(x,t) = \sum_{n=-\infty}^{\infty} c_n e^{i(k_n x - \omega_n t)}, \text{ with } \omega_n = \omega_0 + n\Omega, \; k_n = k_0(1 + n\frac{\gamma}{2}), \qquad (1)$$

In the case under consideration, the phase π -modulation, the coefficients of c_n in eq.(1) are

$$c_n = \frac{2}{i\pi n}, \quad n = 2s - 1. \qquad (2)$$ It is follows from eq.(2) that the waves of the even order including the zero one, which corresponds to the wave with initial energy, were absent in the final state, Only the wave of the first order (with n = –1 during the half of the rotation period and n = +1 during other time) were focused. All other waves were a source of the background. In accordance with eq. (2) the limited possible efficiency of such lens is $|c_1|^2 \approx 0.4$.

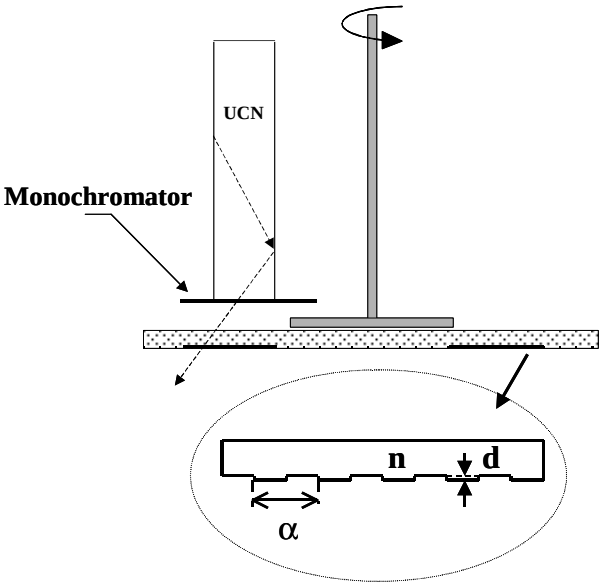

Fig.2. Principle of the experiment. When the grating is spinning, each point of the monochromatic UCN beam is crossed by the moving grating

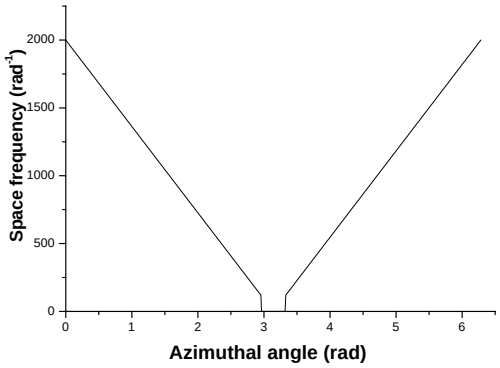

Fig.3. Dependence of the grating space frequency on the azimuth angle at the grating surface

In figure 4 the time-of-flight spectrum obtained in the experiment with rotating grating is represented. The time scale is equal to the rotation period. Rotation frequency is 5820 rpm. It is seen clearly in this figure that moments of the neutron rich detector are not distributed arbitrary but are grouped around some value. Note that the neutron time of flight is about 140 msec, which is 14 time larger than the rotation period.

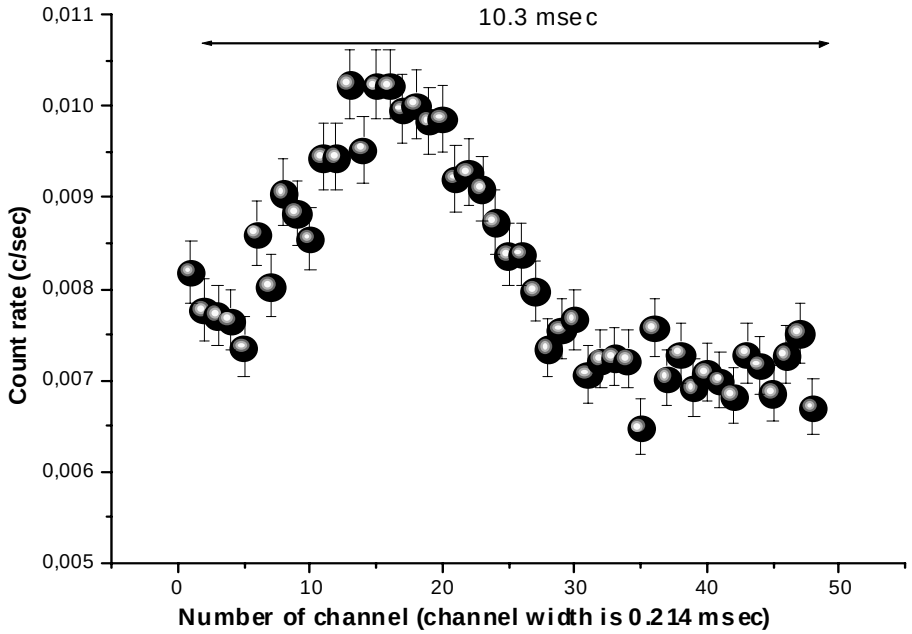

Fig. 4. Time focusing effect

The measurements were done at a number of different rotation frequencies. When the frequency decreases the time scale is also deformed and the visible position of the focusing peak shifts at this scale, respectively. At the same time the width of the peak increases and when the frequency becomes about 2000rpm the focusing effect disappears.

The focusing efficiency was around 17% while it limit value is 40%. Similar intensity of the first order waves was detected earlier in [3,4]. Probably, this deficit in the value of efficiency is due to the quality of grating used in the last experiment, which was not good enough.

References

1. A.I.Frank, R. Gähler. Phys. At. Nucl. **63** (2000), 545.
2. A.I. Frank., V.G. Nosov. Phys.Lett. **A 188** (1994) 120.
3. Frank.A.I., Bondarenko I.V., Balashov S.N. et al. In: VIII International Seminar on Interaction of Neutrons with Nuclei (ISINN-8). E3-2000-192, Dubna, 2000, pp. 448-453.
4. A. I. Frank, S.N.Balashov, I.V.Bondarenko et al. Submitted to Phys.Lett.A
5. I.V.Bondarenko, A.I.Frank, S.N.Balashov et al. NIM **A 440** (2000), 5
6. A. Steyerl, W. Drexel, S.S. Malik, E.Gutsmiedle. Physica **B 151** (1988) 36.

THE REASON FOR SMALL CHANGES IN ENERGY OF ULTRACOLD NEUTRONS (UCN) IN TRAPS

E.V.Lychagin [1], D.G.Kartashov [2], A.Yu.Muzychka [1], V.V.Nesvizhevsky [3], G.V.Nekhaev [1], A.V.Strelkov [1]

[1] *Joint Institute for Nuclear Research, Dubna, Russia*
[2] *National Institute of Nuclear Physics, Pisa, Italy*
[3] *Institute Laue-Langevin, Grenoble, France*

The nature of the phenomenon of small changes in energy of ultracold neutrons (UCN) is investigated. This phenomenon consists in the increasing of UCN energy (heating) by ~10^{-7}eV with the probability of 10^{-8}-10^{-5} per collision with a surface. Such neutrons are named VUCN (vaporized UCN). We found that preliminary outgasing of samples at 500-600 K leads to increasing of the "small heating" probability at least 100 times on a surface of stainless steel and ~10 times on a copper surface. Extremely intensive UCN "small heating" by diamond nanoparticles powder have been observed for the first time. The spectrum of neutrons heated on nanoparticles powder and the temperature dependence of the heating probability are similar to those observed for stainless steel, beryllium and copper. We have observed neither small UCN heating, nor nanoparticles on a mono-crystalline sapphire surface. Thereby the phenomenon of "small heating" can be related to inelastic scattering of UCN by thermal motion of nanoparticles weakly bound to surface.

In 1997, we found an additional channel of losses of ultracold neutrons (UCN) from traps [1]. These losses are due to increase in energy of UCN by ~10^{-7}eV with the probability of 10^{-8}-10^{-5} per collision with surface. If the energy of a neutron after this inelastic scattering exceeds a certain critical value, it leaves the trap. This process is similar to "vaporization" of UCN from trap (see Fig.1). For this reason, such neutrons are named "vaporized" UCN (VUCN).

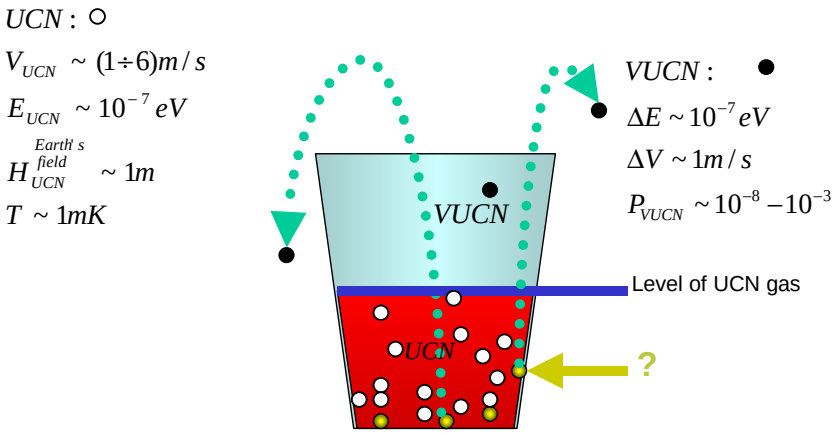

Fig.1 Illustration of losses of UCN from a trap via VUCN production. The typical parameters of UCN (velocity, energy, rising height in the gravitational field, temperature) and VUCN production (change in energy, in velocity, the probability) are shown on the picture.

In order to investigate the nature and characteristics of this phenomenon, we constructed a big gravitational spectrometer (BGS) (see Fig.2).

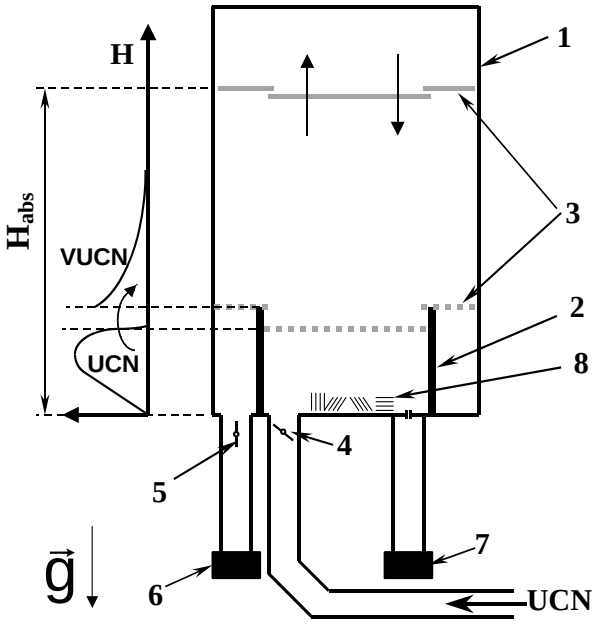

Fig.2 Scheme of the gravitational spectrometer.
1 – evacuated volume; 2 – gravitation barrier;
3 – absorber in upper (solid line) and bottom (dashed line) position ;
4 – input valve; 5 – output valve; 6 – detector; 7 – monitor.

This spectrometer can simultaneously detect stored UCN and formed VUCN. Contrary to previous setups, the BGS provides detection of VUCN in a broader energy range (50-150 neV) and with higher efficiency (~50%). This efficiency is measured rather than estimated over the entire energy range in order to ensure the accuracy and reliability of results. The spectrometer was designed so that samples can be rapidly and conveniently replaced, and the setup can be adapted for various experimental problems. The spectrometer volume hermetically separated from the vacuum enclosure can be heated up to 600 K or cooled down to 80 K. The spectrometer is described in ref. [2]. Fig.3 shows the typical time dependence of the detector count rate with various samples. During filling the spectrometer (0^{th}-100^{th} s), neutrons with energies higher than the gravitational barrier can penetrate into the detector. After closing the input valve (100^{th} s), these neutrons are rapidly absorbed, and the detector count rate falls down for a short time. Then at 170^{th} s, after cleaning the spectrum from above-barrier neutrons, the absorber is lifted up and allows in this position to measure VUCN – neutrons which have changed their energy due to interaction with surface of samples placed in the spectrometer and with the spectrometer walls. The detector count rate rises and, after a certain time, becomes proportional to the flux density of UCN closed by the gravitational barrier in the spectrometer. At the 590^{th} s, the absorber is drawn down**,** and the detector count rate falls down to the background value.

The probability of the small heating of UCN interacting with metal surface (stainless steel, copper) was measured with a higher accuracy by a more reliable method than in previous experiments [1,3,4]. The new measurement confirms our previous results obtained with similar samples for both the probability of this process and for the shape of the integral VUCN spectrum. For the first time, the integral VUCN spectrum was measured with accuracy sufficient for calculating the differential spectrum.

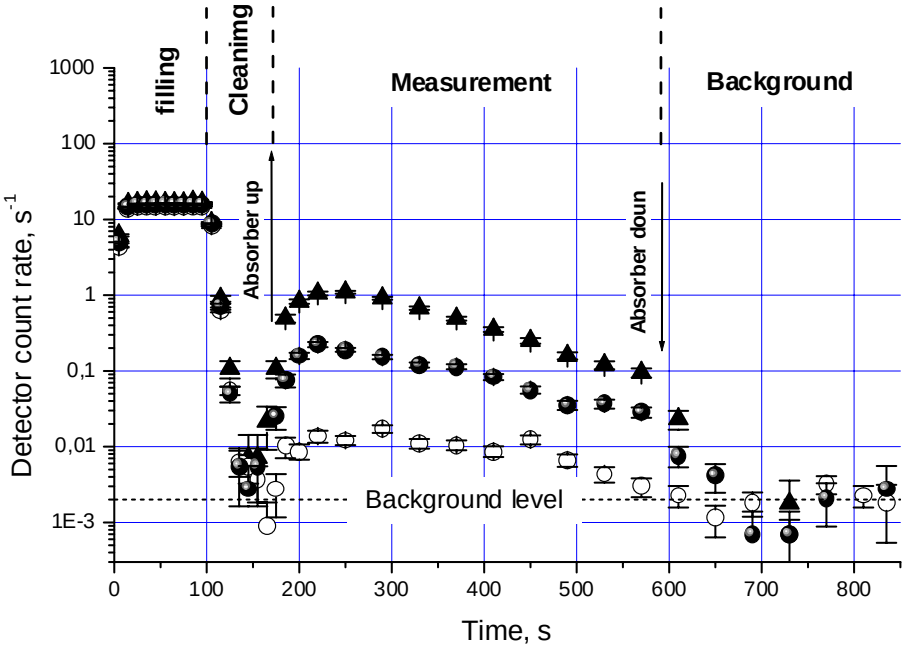

Fig.3. Detector count rates for different samples: measurements (○) on surface of empty copper spectrometer, (●) with stainless steel samples, and (Δ) with diamond nanoparticles powder. The dashed line shows the background level.

We have established that the probability of small heating of UCN depends on the procedure of preparing the stainless steel samples. Indeed, a preliminary heating of sample at the temperature of 500-600 K increases the probability of small heating of UCN by a factor of ~100! The independent measurements with identical samples indicate that this result is well reproducible (see Fig.4). Measurements with an atomic-force microscope showed a big increase in population of nanoparticles at the surface just at this "peak" temperature. The similar abrupt increase in the probability of small heating (by a factor of ~10) after heat treatment was also observed for the interaction of UCN with a copper surface. It should be noted that the preliminary heating of surfaces of traps and samples up to these temperatures is the routine preparatory procedure in UCN storage experiments. Therefore the interpretation of experiments where UCN losses caused by small heating are not explicitly measured is unreliable.

We consider the acceleration of UCN by the thermal motion of solid nanoparticles weakly bound to a surface as the most probable cause of the small heating of UCN [5]. In order to verify this hypothesis, we deposited a powder (~1cm^3) of diamond nanoparticles with a mean size of ~5 nm (Ultradiamond-90) on an area of ~150cm^2 on the copper bottom surface of the spectrometer. In this case, the VUCN flux increased strongly (see Fig.3), and the probability of VUCN production reduced to this area was as high as ~10^{-3} per collision. The VUCN spectra measured in this study and in [1,3,4] on the stainless steel surface coincide with the spectrum measured on the nanoparticles-powder surface. The temperature dependence of small-heating probability measured in the range of 100-300 K for the diamond-nanoparticle powder coincides with the dependencies measured in [3] for the beryllium and copper surfaces. Furthermore, the VUCN spectrum does not significantly depend on temperature in the temperature range 100-300 K.

Whereas we observed a high VUCN flux from the nanoparticles powder, small heating of UCN on the surface of a sapphire single crystal was not detected. The probability of this heating was measured to be $(0.0\pm1.2)\cdot10^{-8}$ per collision. In this case, the scanning atomic force microscope observed no nanoparticles on this surface.

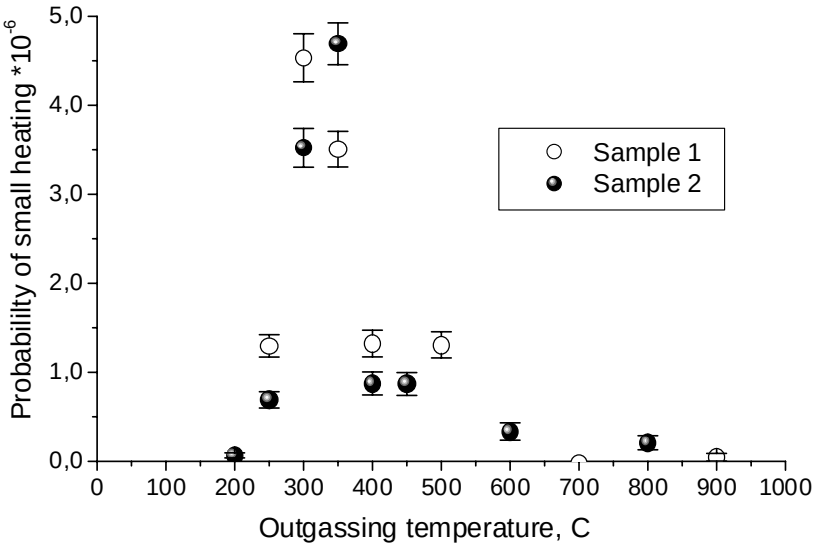

Fig.4. Probability of the small heating of UCN as a function of the outgassing temperature for two stainless steel samples.

The results of this study indicate that the small heating of UCN interacting with a surface is caused by their acceleration in collisions with very small solid particles that are weakly bound to surface and are in permanent thermal motion.

References:

1. V.V.Nesvizhevsky, A.V.Strelkov, P.Geltenbort, and P.S.Yaidjiev, ILL Annual Report (Grenoble, 1997), p.62; European Journal of Applied Physics 6, 151 (1999); Physics of Atomic Nuclei 62, 776 (1999); A.V.Strelkov, V.V.Nesvizhevsky, P.Geltenbort et al, Nuclear Instruments and Methods in Physics Research A 440, 695 (2000).
2. E.V.Lychagin, D.G.Kartashov, A.Yu.Muzychka, V.V.Nesvizhevsky, G.V.Nekhaev, and A.V.Strelkov, Physics of Atomic Nuclei 65 1995 (2002).
3. E.V.Lychagin, A.Yu.Muzychka, V.V.Nesvizhevsky et al, Physics of Atomic Nuclei 63, 548 (2000).
4. E.V.Lychagin, A.Yu.Muzychka, V.V.Nesvizhevsky et al, JINR Preprint R3-2001-49.
5. V.V.Nesvizhevsky, Physics of Atomic Nuclei 65, 400 (2002).

RECENT RESULTS ON THE MEASUREMENTS OF THE P-ODD CORRELATIONS IN THE CAPTURE OF SLOW POLARIZED NEUTRONS BY ^{6}Li AND ^{10}B

Yu. M. Gledenov, P. V. Sedyshev

Frank Laboratory of Neutron Physics, Joint Institute for Nuclear Research, Dubna, Russia

V. A. Vesna, E. V. Shulgina

Petersburg Nuclear Physics Institute of Russian Academy of Sciences, Gatchina, Russia

V. V. Nesvizhevsky, A. K. Petukhov, T. Soldner

Institute Laue- Langevin, Grenoble, France

O. Zimmer

Technische Universität München, Germany

One of the basic predictions of a standard model of the electroweak interaction is the existence of neutral currents. These currents were observed without any ambiguities in the leptonic and semyleptonic processes. However till now the weak neutral current in the NN-interaction is not found out. The major circumstance determining prospects of studying of the P-odd effects in NN-interaction is the possibility of its theoretical interpretation in terms of constants of the NN-potential breaking parity and the nuclear matrix elements which are included in expression of observable P-odd values. The promising direction for the exploration of the properties of neutral currents in the weak NN-processes is the reactions of slow polarized neutrons with light nuclei (A=6-10). These nuclei are well described in cluster and multycluster schemes. Then the task of calculation of the P-odd effects can be solved, using methods, applied for fewnucleon systems. Within the framework of such approach in Ref [1, 2], the P-odd correlations of the triton emission in the ^{6}Li(n,α)^{3}H reaction and the γ-quanta emission at transition from the first excited state of ^{7}Li*$\rightarrow^{7}$Li+γ(M1), E_γ=0.478 MeV, populated in the ^{10}B(n,α)^{7}Li reaction with polarized thermal neutrons, were expressed in terms of weak meson exchange constants. Estimations show, that the possible contribution of neutral currents to the asymmetry values is about 30-50 %. Thus, having measured P-odd correlations and using the values of constants for the charged currents confirmed with experiment, it is possible to obtain an estimation on the contribution of neutral currents to NN-interactions. Expected values of the P-odd correlations are small - $\alpha^{t}_{PNC}\sim 3\cdot 10^{-7}$, $\alpha^{\gamma}_{PNC}\sim 5\cdot 10^{-8}$, however, the high cross sections of the mentioned reactions with thermal neutrons give the possibility to get the P-odd asymmetry with an accuracy of $\sim 10^{-8}$.

The experiments on research of the P-odd asymmetry in the ^{6}Li(n,α)^{3}H and ^{10}B(n,α)^{7}Li*$\rightarrow\gamma\rightarrow^{7}$Li(g.s.) reactions were carried out at the PF1B instrument of the ILL reactor, Grenoble, France. The mean wavelength of the neutron spectrum was $<\lambda_n>$= 4.7 Å. A focusing supermirror polarizer sized the beam of 100 mm in height and 50 mm in width at a focal length (1.8 m). An integral polarized neutron flux was $F_n\sim(3\text{-}5)\cdot 10^{10}$ s^{-1}. The degree of polarization was P=(94±2)%.

The scheme of the experimental setup for the investigation of the ^{6}Li(n,α)^{3}H reaction is represented in fig. 2. The longitudinally polarized neutron beam was used. A geometry of experiment was $\vec{\sigma}_n \| \vec{p}_n \| \vec{p}_t$. To registration of tritons a 48 section ionization chamber was applied. 24 lithium targets were placed along the chamber. The plane of targets was installed

perpendicularly to the beam axis. The targets were the ^{6}LiF layers of 400 μg/cm^2 in thickness, which were prepared by the vacuum evaporation onto the 14 μm Al-backings. In order to absorb the α-particles and to create the needed solid angle for the triton emission, each target from the side of lithium layer was covered additionally also with the 14 μm Al-foil. Each target was common for the "forward" and "backward" detecting sections. As a working gas, argon was used at pressure p = 2.4 atm. The neutron beam was completely stacked in the target area. The targets utilized approximately 60% of the beam intensity. The chamber was supplied with a system of the coils to create needed permanent neutron spin guide magnetic fields. For more details see [3, 4]. The asymmetry coefficient α^t_{PNC} was determined as a relative difference of triton yields along and opposite the neutron spin. For it, the neutron polarization was periodically reversed with the help of a radiofrequency spin-flipper. The signal electrodes of all the "forward" and "backward" sections were connected to the common busbar "forward" and, respectively "backward" to work on two detector channels. The load on the detector was more than 10^9 s^{-1}, due to it the current method of event detection was used. Electronics for the integral measurements are described elsewhere [5]. In order to awoid the possible influence of apparatus instability, neutron flux fluctuations, radiotechnical noises and false effects, the special measurement procedure was used including compensation of the reactor power fluctuations at subtraction of the "forward" and "backward" effects, and the periodical reverse of the guide magnetic field in the chamber [3-6].

In main run for 18 days the P-odd asymmetry was obtained: α^t_{PNC} = -(7.1 ± 3.9)·10^{-8}. In order to estimate the left-right asymmetry contribution, a run was performed, when a guide field was oriented perpendicularly to the neutron beam axes. It was found out that in geometry of the main experiment the contribution of the left-right asymmetry to P-odd effect does not exceed 8·10^{-9}. Beside of this, the background asymmetry measurement was performed without the neutron beam. It allows one to estimate possible influence of the power net noises as well as the scattering electromagnetic fields from the other working facilities in the experimental hall. The result of the background experiment is α_{BG} = (5.6 ± 4.3) 10^{-9}. The "zero" experiment with total absorption of tritium component was not done due to lack of the beam time. However, the background effect is expected to be no more than in the previous experiment [7] - α_0 = (2.1 ± 1.7)·10^{-8} (see discussion in [3, 4]).

Using the obtained value and results of the previous experiment in Gatchina [7] it is possible to estimate a meson exchange constant of the weak neutral current. A sum of the P-odd coefficients of the present experiment and [7] (weighted averaged) gives α^t_{PNC} = -(7.1 ± 3.3)·10^{-8}. Assuming, that the charged current constant is known exactly h_ρ = -11.4·10^{-7}, and using expression from [1] we obtain $f_\pi \le 1.2\cdot10^{-7}$ at the 90% confidential level. At present, this estimation of the neutral current constant is the most accurate among others.

First experiment on the measurement of the P-odd correlation in the ^{10}B(n,α)^{7}Li*→γ→^{7}Li(g.s.) reaction was performed in 2001 [8]. The main run gave the asymmetry coefficient α = + (8.8±4.6)·10^{-8}. The "zero"-experiments showed a significant background effect with the sign opposite to the sign of the main run value: α_0 = -(14.8±3.3)·10^{-8}. In the experiment of 2002 essential part of efforts was concentrated on understanding of the nature of background effect. Number of runs were carried out to investigate construction materials of the facility and the samples. It has been established, that the sample, used in first experiment for the 0-measurements, was locally contaminated, probably, with chlorine, that gave big background effect. The main results of recent experiment are as follow: the ^{10}B run - α = -(11.0 ± 6.6)·10^{-8}, the 0-experiment - - α_0 = (0.7 ± 3.7)·10^{-8}. From the comparison wit theoretical calculation (α^{theor} = -7.24·10^{-8}) it is seen, that experimental accuracy still is not enough to make the estimation of the neutral current contribution.

At present, the feather measurements are in the stage of planning. Use of new improved polarizer gives the real possibility to increase experimental accuracy in factor of 2-3 and to get the P-odd effect values with uncertainty of ~1-1.5·10^{-8}.

This work is supported by the Russian Foundation for Basic Research, Grant No. 00-02-16707.

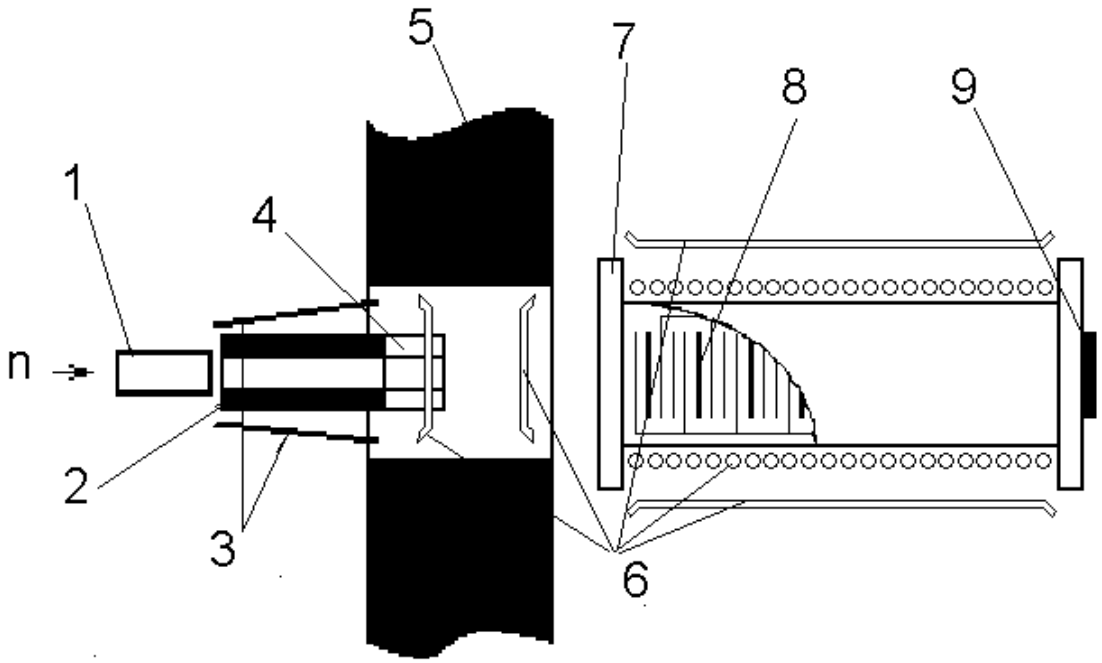

Fig. 1. The experimental layout for the ^{6}Li mesurements: 1- polarizer; 2- adiabatic RF spin-flipper; 3- magnetized plates of the neutron spin guide field; 4- lead collimator; 5- concrete wall; 6- coils of the neutron spin guide field; 7- ionization chamber; 8- targets and electrodes; 9- Li beam-stop.

References:

1. N. N. Nesterov, I. S. Okunev. JETP Letters 48 (1988) 573.
2. V. A. Vesna, Yu. M. Gledenov, P. V. Lebedev-Stepanov, I. S. Okunev, A. V. Sinyakov, Yu. M. Tchuvil'sky, E. V. Shul'gina. Phys. At. Nucl. 62 (1999) 522.
3. Yu. M. Gledenov, V. A. Vesna, V. V. Nesvizhevsky, A. K. Petukhov, P. V. Sedyshev, T. Soldner, E. V. Shulgina, O. Zimmer. JINR Communication. P3-2002-151 (Dubna 2002).
4. V. A. Vesna, Yu. M. Gledenov, , V. V. Nesvizhevsky, A. K. Petukhov, P. V. Sedyshev, T. Soldner, E. V. Shulgina, O. Zimmer. PNPI Preprint. No. 2479 (Gatchina 2002).
5. V. A. Vesna, E. V. Shul'gina. PNPI Preprint No. 2425 (Gatchina 2001).
6. Yu. M. Gledenov, I. S. Okunev, S. S. Parzhitskii, E. V. Shul'gina, V. A. Vesna. NIM A350 (1994) 517.
7. V. A. Vesna, Yu. M. Gledenov, I. S. Okunev, Yu. P. Popov, E. V. Shul'gina. J. Nucl. Phys. 59 (1996) 23.
8. V. A. Vesna, Yu. M. Gledenov, V. V. Nesvizhevsky, A. K. Petukhov, P. V. Sedyshev, T. Soldner, E. V. Shulgina. Izvestija Academii Nauk. Ser. Fiz. 67 (2003) 118-122

ON THE RELIABILITY OF THE MODEL-INDEPENDENT EXTRACTION RESULTS OF THE LEVEL DENSITY AND RADIATIVE STRENGTH FUNCTIONS FROM THE *(N, 2γ)* REACTION

A.M. Sukhovoj, V.A. Khitrov

Joint Institute for Nuclear Research, Dubna, Russia

Until recently level density (LD) $p = D^{-1}$ and radiative strength function (RSF) $k = \Gamma_{\lambda i} /(E^3_\gamma \times A^{2/3} \times D_\lambda)$ E1- or M1-transition with the energy E_γ and mean width $\Gamma_{\lambda i}$, connecting λ and *i* states in the excitation range from $E_{воз} \cong$ 1- 2 MeV to the neutron binding energy B_n in the nucleus with mass A were derived only from evaporative spectra of the (p, n) reaction type and primary γ-transition spectra, respectively. The main shortage of the mentioned methods is the necessity to use purely model notions about the penetration of the nucleus surface for evaporative nucleons [1] or level density in determination of RSF [2].

The situation changed when authors [3] showed that total radiative width $\Gamma_\lambda =< \Gamma_{\lambda i} > \times m_{\lambda i}$ and two-step cascade intensity $I_{\gamma\gamma} = \Sigma_{J,\pi}(\Gamma_{\lambda i} / < \Gamma_{\lambda i} > m_{\lambda i}) \times n_{\lambda i} \times (\Gamma_{if} / < \Gamma_{if} > m_{if})$ connecting compound state λ with the given low-lying levels of nucleus *f* and exciting at the same time $n_{\lambda i} = \rho_i \Delta E$ intermediate states *i* from any interval of ΔE width can be reproduced in calculation within the experimental precision. This circumstance allowed us to obtain unique information about ρ and *k*, as an infinite number of possible DL and RSF (each of which allows to reproduce Γ_λ and $I_{\gamma\gamma}$ accurately) lies in a very narrow interval of their value variation for any of γ-quantum energy and nucleus excitation $E_{воз} < B_n$.

Methods [3] have 2 most important sources of error in determination of ρ and *k*:

a) the error in determination of the $I_{\gamma\gamma}$ absolute value and

b) the error in separation of experimental spectrum of two-step cascades into two symmetric parts, which depend on energy of only primary E_1 and only secondary E_2 cascade transition.

The error in determination of intensity is easy to control, if a large statistics of useful events allows one to determine peak areas in the sum coincidence spectrum of cascades to the final levels with the excitation energy E_f not less than $\approx 0.5\ B_n$. Their simple correction for registration efficiency and probability of the useful coincidence loss easily available for experimental determination because of the third and subsequent quanta of cascades registration allows to determine the sum of cascade intensities and direct transitions to the lowest cascade levels. This sum may exceed 100% only if $I_{\gamma\gamma}$ is too high. Its experimental value varies from ≅ 70% for W isotopes to ≅ 90% for *Os* isotopes with the value of $2.0 < E_f < 2.5$ MeV, respectively. On the basis of these data and different model calculations we can assume that relative errors in determination of $I_{\gamma\gamma}$ are of the same scale as errors in determination of the sections of thermal neutron capture (10-20%).

All measured in the experiment distributions of cascade intensities represent a superposition of a certain number of pairs of peaks having different intensity and “noise” line with zero mean value (the result of background subtraction). That is why, at a rather high statistics of coincidence from any spectrum of two-step cascade connecting compound state and given low-lying level, it is practically possible to extract even in any deformed nucleus several hundreds of pairs of resolved intense peaks, which corresponds to 90 and more per cents of cascade intensity with the energy of their intermediate level less than $\leq 0.5\ B_n$. Using the maximum likelihood method for these cascades it is possible to determine [6] γ-ordering in cascade. At the same time the energies of nucleus levels are defined with a rather high degree of reliability and the transitions are placed in the γ-decay scheme.

Then the intensities of the cascades with primary transitions and with energy $E_1 > 0.5B_n$ placed [6] in the decay scheme are subtracted [4] from experimental spectra. The remaining part of

spectrum is, basically, a superposition of intensities of a large number of cascades with primary transition energy less than $0.5B_n$ and "noise" distribution with zero mean. Since there exists a non-zero threshold of cascade intensity $i_{\gamma\gamma}$ with primary transitions and energy $E_1 > 0.5B_n$, the intensity and quantum energies of which can be derived from spectrum, the procedure [4] may slightly overstate the value of total cascade intensity with $E_1 < 0.5B_n$ and, consequently, understate it for the equal value for symmetric energies of cascade quanta.

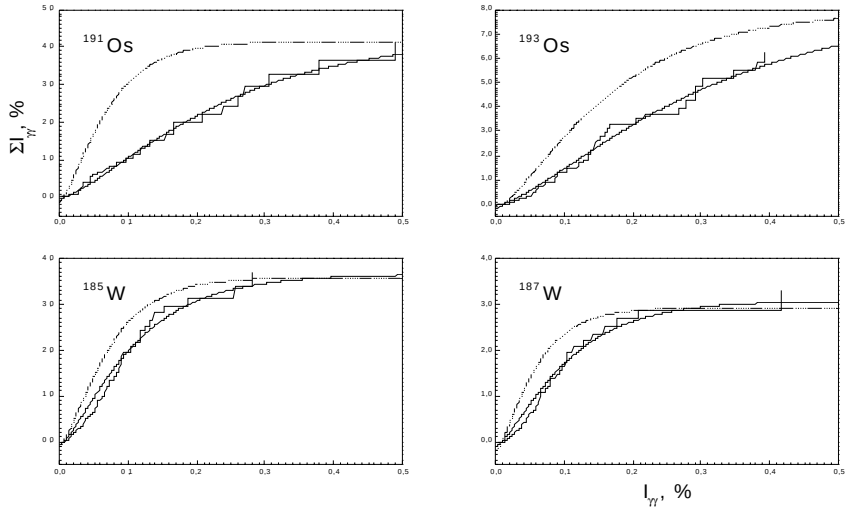

Fig. 1. Cumulative sums of $I_{\gamma\gamma}$ intensity experimentally observed in ^{185,187}W and ^{191,193}Os cascades (histogram) for the energy interval of their intermediate level from 2.5 to 2.75 MeV (% of compound state decays), the approximated dependence (solid line) and the expected one for number of levels, predicted by model [11] (dot line) for the same total cascade intensity.

The estimation of maximum relative value of the error in question does not exceed several per cents for the last experiments carried out at the spectrometer of high efficiency coincidences in Rez [8]. This can be seen on fig. 1 showing an example of approximation [9] of cumulative sums of all cascade intensities populating one and the same intermediate level in the interval near $0.5B_n$ of excitation energy for four nuclei under consideration: ^{185,187}W and ^{191,193}Os. Similar data were obtained for lower excitation energies. Module of extrapolated dependence for $i_{\gamma\gamma} = 0$ determines the expected absolute value of intensity for low-intensity cascades with energy of their intermediate level within the mentioned interval of values.

As follows from the data analysis of such type for other intervals below $0.5\ B_n$, in modern experiments the intensity part of low-intensity cascades with $E_1 > 0.5B_n$, which were not extracted from spectrum and, thus, not placed in the decay scheme, does not exceed $\cong$ 1% if only the deviation of primary transition intensities from the mean value is described by the Porter-Thomas distribution [10] (or by any other one with smaller dispersion).

The error of such scale, as seen from modeling, does not introduce any principle changes into the obtained, in accordance with [3], energy dependences of LD (fig. 2) and RSF (fig. 3). Such verification was performed under the assumption that cascade intensities are overestimated by 50 % in the analyzed nuclei. The result of modeling is given in the same figure for comparison.

New and, apparently, the most precise for today experimental data concerning two-step cascades in W and Os isotopes confirmed the necessity for improvement in theoretical description of nuclear properties in the region of transition from "simple" states at $E_f \leq$ 1-2 MeV to the very complicated states (for example, to neutron resonances). Observation of the step-like change in the dependence of LD confirms the conclusion made in [3] about the irrelevance of notions of "smooth" changes in nuclear properties during the transition from "order" to "chaos".

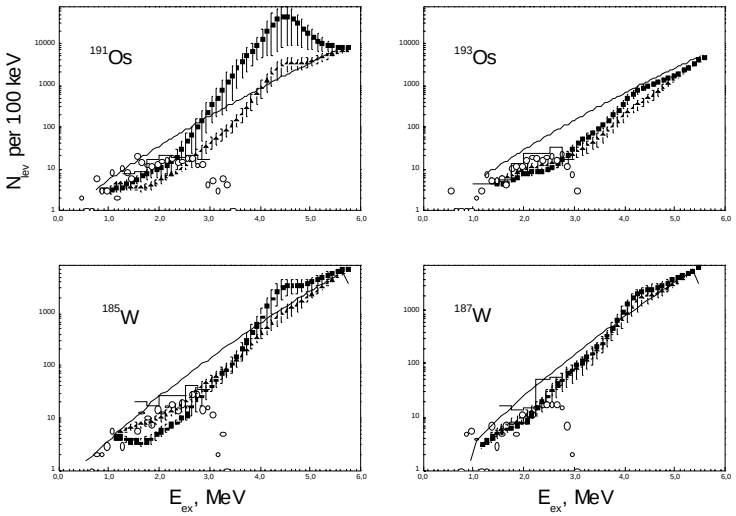

Fig. 2. Number N of levels of both parities excited by dipole primary transitions. Circles represent a number of experimentally observed intermediate levels of two-step cascades, histogram represents their most probable expected values for zero threshold of cascade registration [9]. Points with error bars show the most probable values reproducing Γ_λ and $I_{\gamma\gamma}$. Lines represent calculations according tomodel [11]. Triangles represent the mean value of LD reproducing the values of $I_{\gamma\gamma}$ from fig.1 diminished 1.5 times.

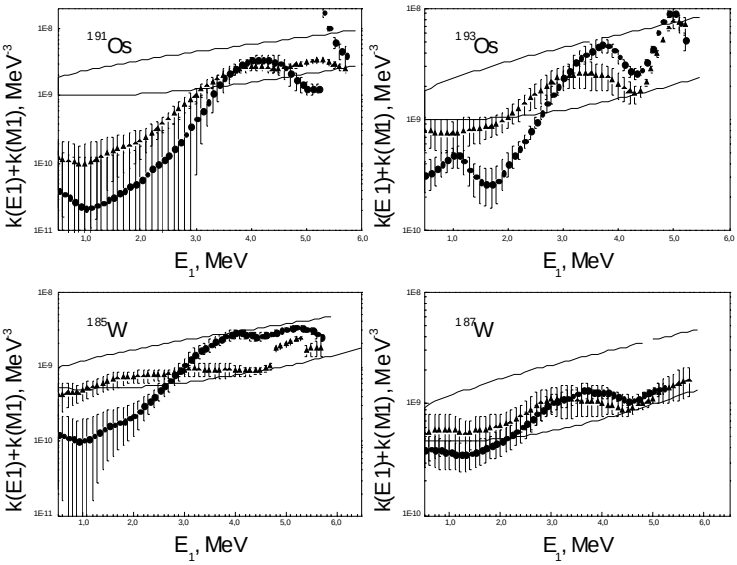

Fig. 3.The most probable sum of strength functions k(E1)+k(M1) of E1 and M1 transitions of radiative thermal neutron capture with its calculated error in the function of the cascade E_1 primary transition energy. Solid lines represent the data of model notions [12, 13] summed with the normalized to experiment value k(M1) = const. Triangles show the same as in fig. 2 for RSF.

The reliable experimental data obtained recently on the parameters of cascade γ-decay process of excited states from the excitation energy region $E_{ex} \cong B_n$ show, at the least, that conventional notions of the nuclear properties below B_n need rather serious correction and further development. And the statistic character notions of γ-decay process evidently fail to provide the reproduction of its experimentally measured parameters within the precision achieved in experiment. The appropriate "statistic" approach leads to underestimation of nucleus structure influence on the parameters, that determine this process, either for the whole interval of B_n excitations, or for its greater part.

STUDY OF ELEMENT COMPOSITION OF *ARTHROBACTER OXYDANS* BY EPITHERMAL NEUTRON ACTIVATION ANALYSIS

M.V.Frontasyeva, S.S.Pavlov, S.F.Gundorina,
L.M.Mosulishvili[1], Ye.I. Kirkesali[1], N.Ya.Tsibakhashvili[1], H.-Y. N. Holman[2]

Frank Laboratory of Neutron Physics of the Institute for Nuclear Reserch, Dubna, Russia
[1]E. Andronikashvili Institute of Physics of the Gorgian Academy of Sciences, Tbilisi, Georgia
[2]Center for Environmental Biotechnology, Lawrence Berkeley National Laboratory, Berkeley, CA, USA

Arthrobacter species are the members of the actinomycete-coryneform bacteria [1]. *Arthrobacter oxydans (A.oxydans),* isolated from Columbia basalt rocks of U.S. DOE contaminated site was identified as Gram-positive Cr(VI) -reducing bacterium by Holman at al. [2]. The ability of bacteria in heavily contaminated sites to survive through the reduction of highly toxic Cr(VI) to less toxic Cr(III) has created significant opportunities to detoxify environment [3].

The purpose of this investigation on the initial stage is to determine the baseline chemical composition of *A. oxydans* using epithermal neutron activation analysis (ENAA) and to study Cr(VI) and Cr(III) uptake by *A. oxydans.*

A. oxydans biomass for ENAA was cultivated in the following nutrient medium: 10 g/l of glucose, 10 g/l of peptone, 1 g/l of yeast extract, 2 g/l of caseic acid hydrolysate and 6 g/l of NaCl. To perform chromium accumulation test *A. oxydans* was kept in the nutrient medium described in [4] and Cr(VI) (as K_2CrO_2) or Cr(III) (as $Cr(CH_3COOH)_3$) was added to the nutrient medium within a concentration range of 10-200 mg/l in the exponential phase of growth. After being cultivated for 5 days the cells were harvested by centrifugation and rinced twice. This wet biomass was dried according to the procedure reported in [5]. The dry native biomass was finally pelletized using a titanium mould.

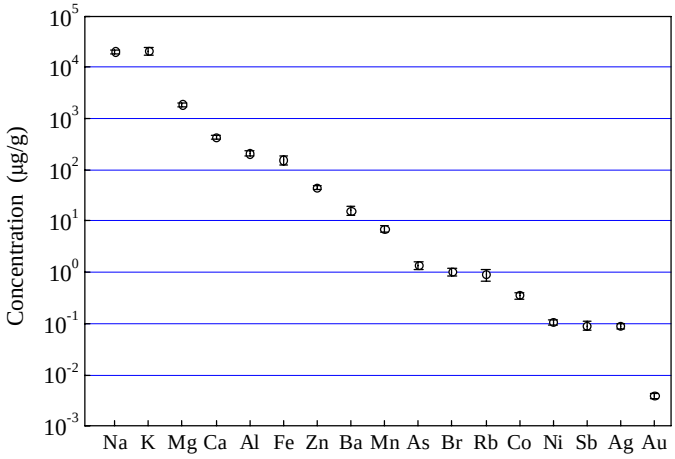

Fig. 1. Elemental distribution in lyophilized samples of A.

ENAA of these samples was carried out at the IBR-2 pulsed fast reactor in FLNP, JINR, Dubna. The ENAA technique for biological samples is described in detail in [5,6]. A total of 17 major, minor and trace elements were determined in the biomass of *A. oxydans* (Fig. 1). As it is seen, the concentration range spans more than 8 orders of magnitude. The increased concentrations of Na and K in the samples are due to biomass being freeze-dried in a Na-K phosphate buffer. The concentrations of Mg, Al, Ca and Fe were found to be high. So, it can be supposed that the composition of *A. oxydans* reflects the chemical composition of the environment to wich it was

confined. The Columbia basalt samples from the studied site are fine-grained silicat rocks and magnetite is also often present [2].

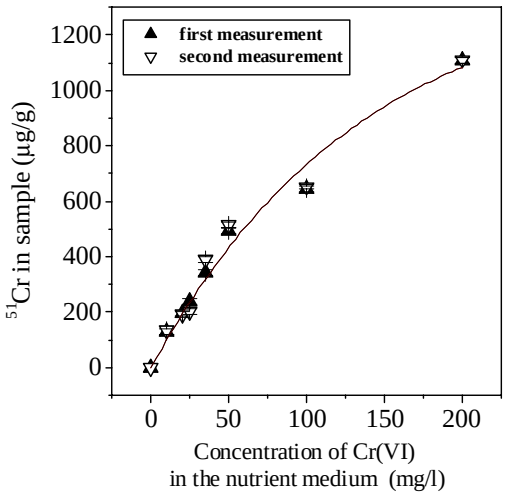

Fig. 2. Chromium content in A.oxydans cells versus Cr(VI) content in the nutrient medium.

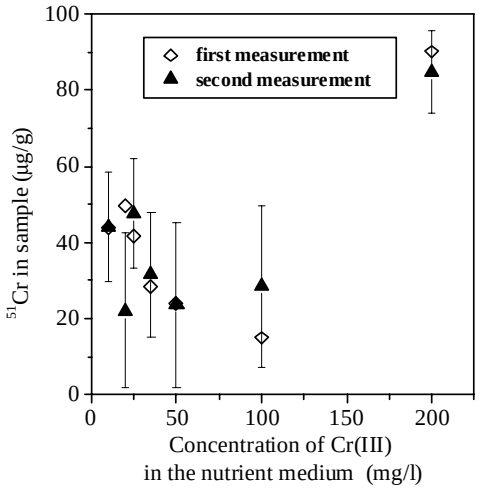

Fig. 3. Chromium content in A.oxydans cells versus Cr(III) content in the nutrient medium.

In Fig. 2 and Fig. 3 the results obtained for samples with Cr(VI) and Cr(III) loading are presented. As it follows from Fig. 2, the total content of intracellular chromium always increases, while the uptake of Cr is more intensive in the interval of Cr(VI) concentrations 10-50 mg/l. At 50 mg/l load (during 5 days) the accumulated chromium is about 500 µg/g. It should be noted that, when Cr(VI) concentration exceeds 50 mg/l , the survival ability of *A. oxydans* cells decreases dramatically [4].

Fig. 3 shows that in the investigated range of concentrations the accumulation of Cr(III) in bacterial cells practically does not take place. However, at a concentration of 200 mg/l Cr content in *A. oxydans* cells increases.Taking into account that the rate and extent of chromium penetration into cells dependens on its extracellular concentration and exposure time, one can assume, that at the concentration 200 mg/l (after 5 days of exposure to Cr(III)) the number of certain complexes of chromium, that have high penetration ability, increases.

The obtained results can be of use for the future investigation of the Cr(VI)-reducing processes in *A. oxydans* and also will be compared with data for other Cr(VI)-redusing endolithic (rock/mineral inhabiting) bacteria.

References:

1. J. Loveland-Curtze, P. Sheriden, K. Gutshall ,J. Brenchley. Arch. Microbiol. 171 (1999) 355.
2. H.-Y. N. Holman, D. Perry, M. Martin, G. Lamble, W. McKinney & J. Hunter-Cevera, Geomicrobiology J. 16 (1999) 307.
3. J. R. Lloyd & D. R. Lovley, Curr. Opin. Biotech. 12 (2001) 248.
4. N. Tsibakhashvili, M. Abuladze, N. Asatiani, N, Bakradze, H.-Y. Holman, T. Kalabegishvili, T. Kartvelishvili, A. Rcheulishvili, N. Sapojnikova & L. Mosulishvili, "Chromium reduction by *Arthrobacter oxydans"*, in: A. S. Kungolos, G. P. Korfiatis (eds.), Proc. Intern.Conf. – Protection and Restoration of the Environment VI**,** Skiathos, Greece, 2002, p. 755 .
5. L.M. Mosulishvili, E.I. Kirkesali, A.I. Belokobilsky, A.I. Khizanishvili, M.V. Frontasyeva, S.S. Pavlov, S.F. Gundorina, J. of Pharmaceut. and Biomed. Analysis, 30 (2002) 87.
6. M.V. Frontasyeva, E. Steinnes, Proc. Intern. Symp. on Harmonization of Health Related Environmental Measurments Using Nuclear and Isotopic Techniques, Hyderabad, India, 4-7 November, 1996, IAEA 1997, p.301.